# Results of STEREO/WAVES antenna calibration, using a refined spacecraft model (Design 1)

Oswald, T.O.,W. Macher, G. Fischer, H.O. Rucker

July 13, 2005

**Abstract**

After receiving accurate information about the STEREO spacecraft, we built a refined wiregrid model to get more accurate predictions about the characteristics of the SWAVES antennas. During this analysis we did the most accurate modeling that is possible with the Matlab ASAP toolbox. The results are presented in this report, which is to be seen as continuation of [1].

# Contents

# Part I
# Spacecraft A

## 1 The revised spacecraft

### 1.1 Change of characteristics

The biggest change, we had to perform is the change of the spacecraft coordinate system. The used reference frame is defined in a way that it is spacecraft fixed with the positive x-axis in a direction which will point to the sun during most of the time, so the antennas are mounted on the side of the hull that points to the negative x-axis. The solar panels point to the positive and negative y- axis and the z-axis is defined in a way that it completes the right handed cartesian frame.

For the description of the direction of the antennas we chose to employ a spherical polar system which has the positive X-axis as polar axis. The angle $\zeta$ is the angle between the positive X-axis and the antenna, and $\xi$ is the azimuthal angle around the X-axis, where E1 is defined to have $\xi = 0$.

There are minor changes in the configuration of the antenna feeds, which we had to include in our new model, and we were informed about the existence of two low gain antennas, we had to include. The identifiers of the ASAP antennas are now E1, E2 and E3 as used by JPL, and they correspond to the antennas A1, A2 and A3 of our first model. The location of the boom was changed. JPL gave us the required information about the base capacitances of antennas, coax cables and receivers. With this information, we were able to calculate and include the base impedances at the second run of the computations. The actual values are tabulated in Table 1.

Table 1: Base Capacitances of the STEREO WAVES antenna system

| **Antenna** | **E1** | **E2** | **E3** |
|---|---|---|---|
| **Antennas/pF** | 55 | 55 | 55 |
| **Receivers/pF** | 25 | 25 | 25 |
| **Cables/pF** | 10 | 10 | 10 |
| **Entire Capacitance/pF** | 90 | 90 | 90 |

The asymmetry of the solar panels is more pronounced than in our first model. Spacecraft A has only one ring mounted on the hull, while spacecraft B has two. Otherwise the two spacecraft are more similar then expected. They are almost identical and differ only by a few differences of their instruments.

### 1.2 The model

For our design 1 studies, we did not model different boom configurations, but built both spacecraft separately and tried to include the most pronounced

differences. The boom is similar to the one of the model with the segmented boom of the preliminary studies. (see figures 1-4).

# 2 The quasistatic regime

## 2.1 Computation of the effective length vectors

Again, the first step was to compute the currents at frequencies from 100kHz to 16MHz, with a spacing of 100kHz with the ASAP program, each frequency with a selection of 19 different angles of the HGA dish. The range of the HGA dish can be seen on figure 5. The impedances were not included at this point, so we still calculated with open feeds. This time, the current system of all frequencies was saved to a single file, but each HGA angle had its own.

# 3 Calculations

Figures 6-8 show plots of the effective length vectors . The frequency used for these plots is 500kHz, being well in the quasistatic regime. The direction of the incident wave is from the positive x-axis, simulating radiation from the sun.

The following table shows the directions and lengths of the electric and physical antennas at a frequency of 500kHz. The direction to the origin of the wave is, again, the positive x-axis. For comparison, the values of the model from design 1 is included.

Table 2: Effective length vectors at 500kHz

| | | Design 1 | Design 0 | Physical antennas |
|---|---|---|---|---|
| E1 | length/m | 2.80 | 2.26 | 6.00 |
| | $\zeta/°$ | 135.5 | 140.5 | 125.26 |
| | $\xi/°$ | 20.1 | 24.0 | 0.0 |
| E2 | length/m | 4.38 | 3.87 | 6.00 |
| | $\zeta/°$ | 120.9 | 122.2 | 125.26 |
| | $\xi/°$ | 127.1 | 129.7 | 120.0 |
| E3 | length/m | 3.49 | 3.15 | 6.00 |
| | $\zeta/°$ | 128.5 | 129.3 | 125.26 |
| | $\xi/°$ | -142.5 | -147.8 | -120.0 |

The reason for the change of direction of the effective height is most probably the shift of the HGA antenna in direction of the positive X-axis, which is also the reason for the change in $\xi$ of E3. The change in position of the solar panels may also take part in this effect.

## 3.1 Variation of the effective length vectors with frequency and direction

The variability of the real part of the effective length vectors is shown on figures 9-11. The plot was constructed by choosing 26 different directions and

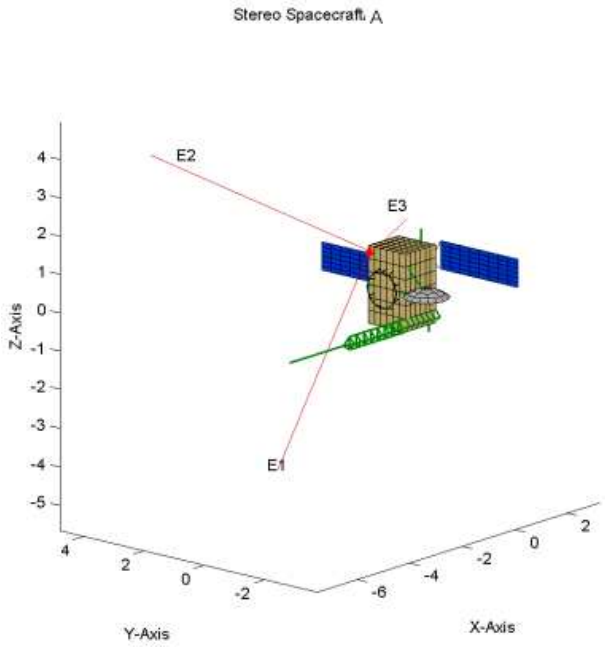


Figure 1: Spacecraft A

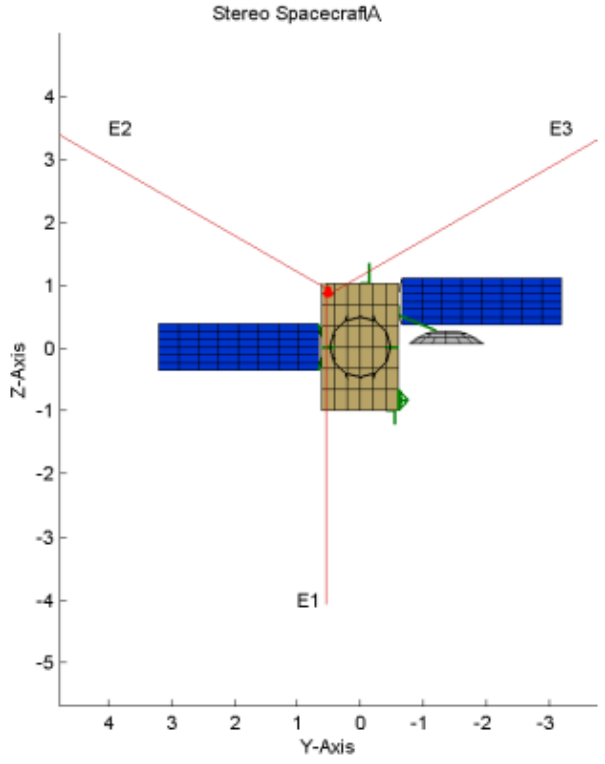


Figure 2: Spacecraft A: View from the negative X-axis

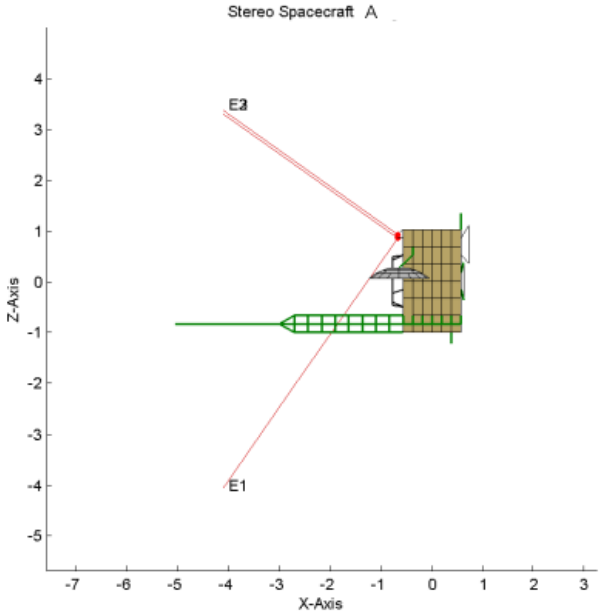


Figure 3: Spacecraft A: View from the negative Y-axis

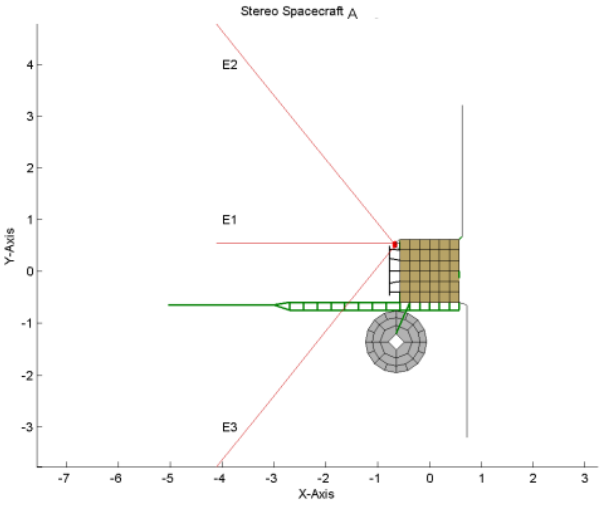


Figure 4: Spacecraft A: View from the negative Z-axis

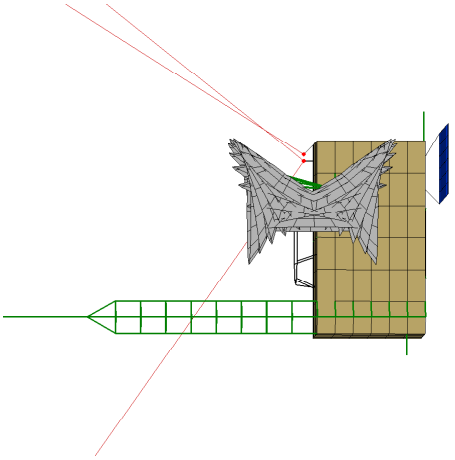

Figure 5: Range of HGA angle

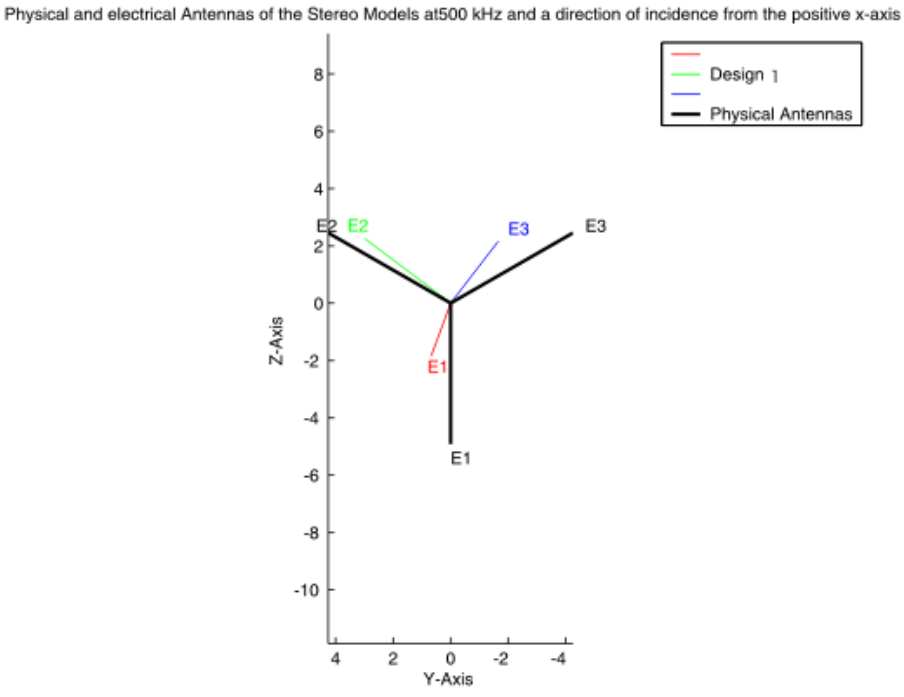


Figure 6: Spacecraft A: Effective Length Vectors, X-View

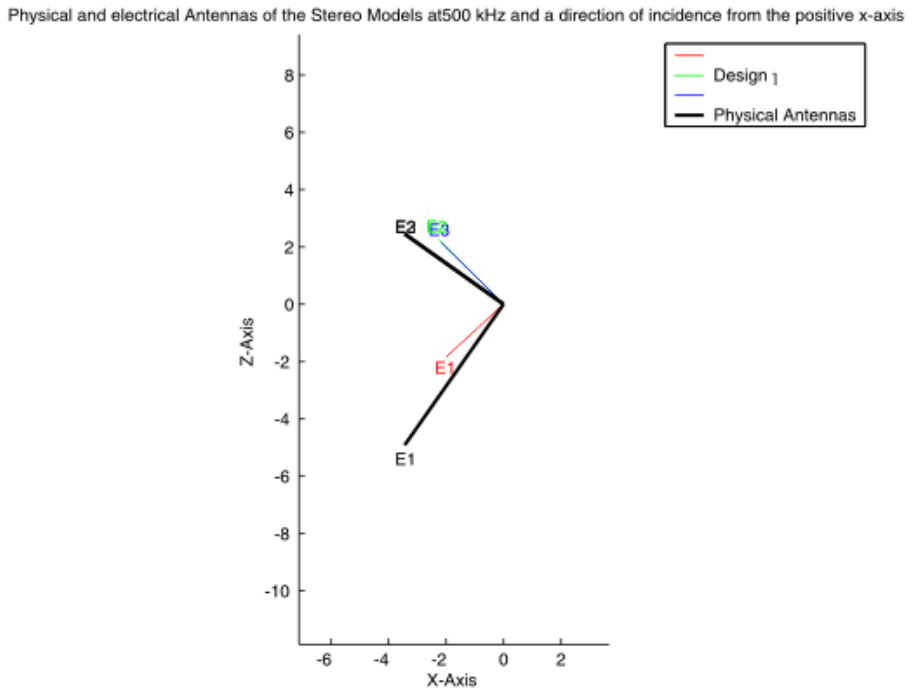


Figure 7: Spacecraft A: Effective Length Vectors, Y-View

computing the effective length vectors for each frequency and each direction. The real part of all effective length vectors were plotted, while the imaginary parts were ignored. The frequency is color coded. The 26 sample directions are shown in figures 12 and 13 for reference. We did not include diagrams of the X- and Y-view, because they look exactly the same as the Z-view.

As method to quantify these plots, we computed the standard deviation of the magnitudes of the length of the effective height vectors, and used the method of the complex Macher Angle, as described in [1]. As a measure of angular distribution the following angle-like value was computed:

$$\sin(\frac{\Delta\alpha}{2}) = \frac{1}{2}\sqrt{\frac{1}{N}\sum_i |\hat{\mathbf{h}}_i - \hat{\mathbf{h}}_0|^2} \tag{1}$$

where $\hat{}$ denotes the corresponding unit vector (in general $\hat{\mathbf{a}} = \frac{\mathbf{a}}{|\mathbf{a}|}$)

This angle has a similar meaning as the standard deviation of the angular distance from the mean of all vectors when the vectors are real.

When DF is regarded to be possible with a knowledge of the directions of the electric antennas with an accuracy of 2 degrees, the graphs dictate an upper limit

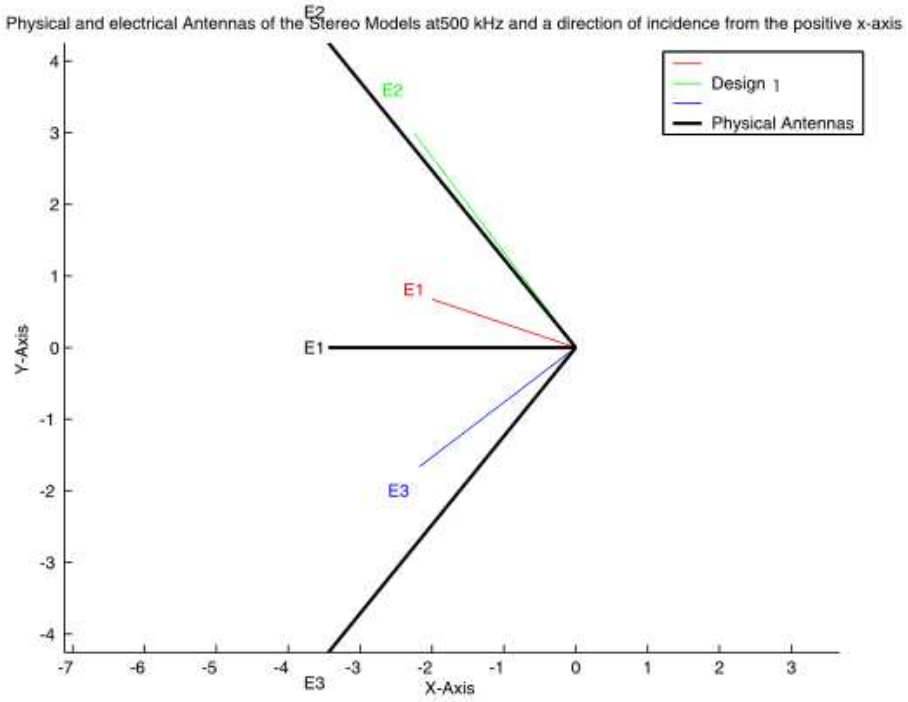


Figure 8: Spacecraft A: Effective Length Vectors, Z-View

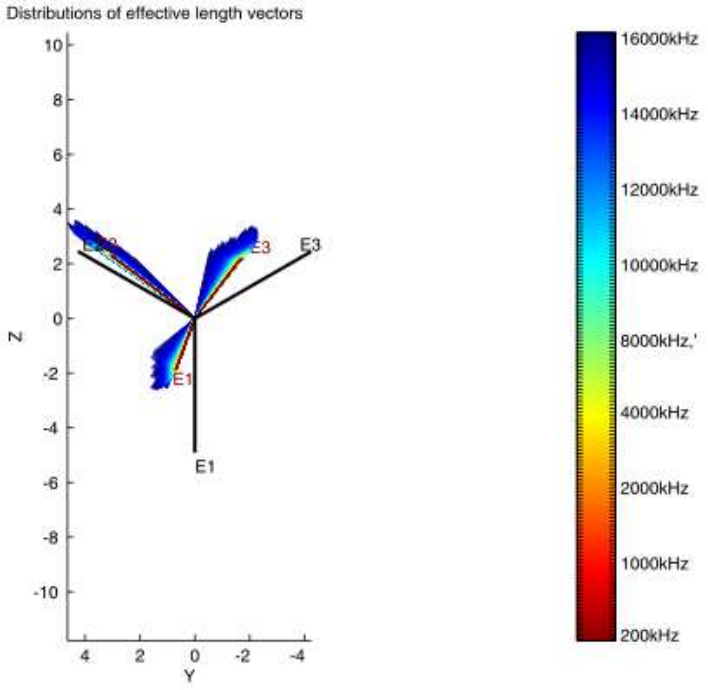


Figure 9: The spatial distribution of the real parts of the effective length vectors of the design 1 model/X View

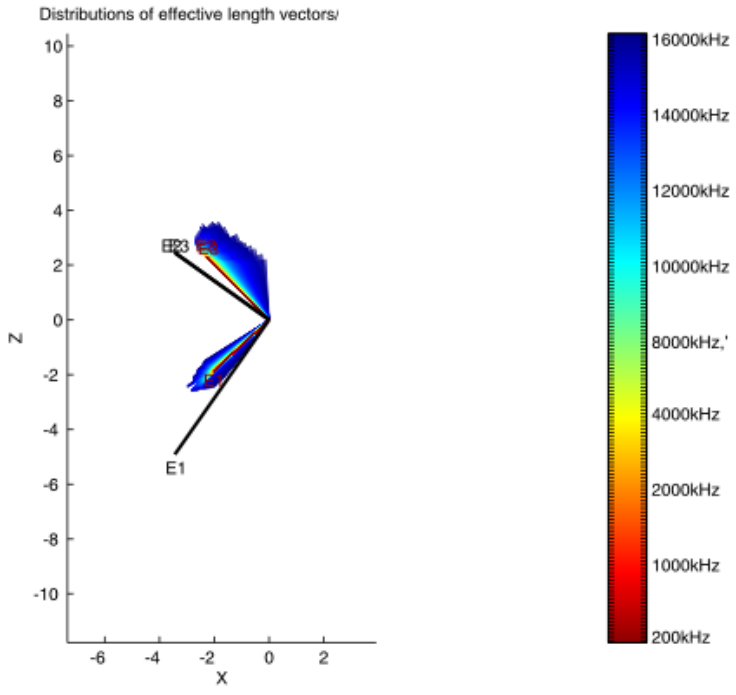


Figure 10: The spatial distribution of the real parts of the effective length vectors of the design 1 model/Y View

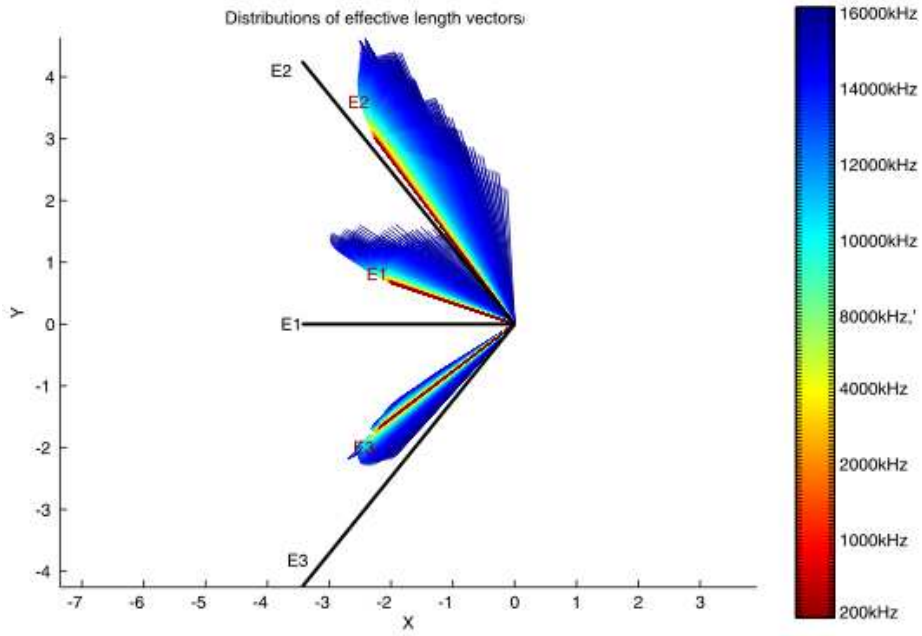


Figure 11: The spatial distribution of the real parts of the effective length vectors of the design 1 model/Z View

of 1.2MHz (see fig. 15). Again, the constraints due to the standard deviation of the antenna effective lengths seem to be less restrictive.

## 3.2 The Covariance Matrix

When performing direction finding, it is useful to know the covariance matrix. (see [3]) We have written a matlab routine to compute the matrix. The formula for the elements of the matrix is

$$\sigma_{u,v} = \frac{1}{N-1}\sum_{i=1}^{N}(u_i - \bar{u})(v_i - \bar{v}) \tag{2}$$

where the diagonal elements are the variances and the other elements are the covariance that describe the interaction of the parameters. One would expect the variances to be larger than the covariances, which is reflected in the actual matrix below. The order of the parameters is
$h_{eff}(E1), h_{eff}(E2), h_{eff}(E3), \xi(E1), \xi(E2), \xi(E3), \zeta(E1), \zeta(E2), \zeta(E3)$ and the units used are meter for the first three parameters and degree for the remaining 6. For frequencies of 500kHz and 1MHz, the results are:

$$10^{-8} \cdot \begin{pmatrix} \mathbf{8.562} & -6.276 & -8.706 & -71.24 & 9.702 & -62.67 & -37.67 & -15.10 & -5.320 \\ -6.276 & \mathbf{55.21} & -7.212 & 59.66 & -85.31 & -48.44 & 49.1 & 70.21 & 22.44 \\ -8.706 & -7.212 & \mathbf{24.89} & 75.16 & 7.221 & 172.7 & 28.41 & -4.143 & -3.813 \\ -71.24 & 59.66 & 75.16 & \mathbf{618.4} & -97.64 & 526.1 & 340.9 & 144.1 & 68.42 \\ 9.702 & -85.31 & 7.221 & -97.68 & \mathbf{134.1} & 50.87 & -79.49 & -109.5 & -37.80 \\ -62.67 & -48.44 & 172.7 & 526.1 & 50.84 & \mathbf{1209} & 192.6 & -30.70 & -38.51 \\ -37.67 & 49.14 & 28.41 & 340.9 & -79.49 & 192.6 & \mathbf{205.9} & 105.7 & 59.24 \\ -15.11 & 70.27 & -4.143 & 144.1 & -109.5 & -30.70 & 105.7 & \mathbf{102.5} & 43.94 \\ -5.320 & 22.44 & -3.813 & 68.41 & -37.80 & -38.51 & 59.24 & 43.94 & \mathbf{36.02} \end{pmatrix} \tag{3}$$

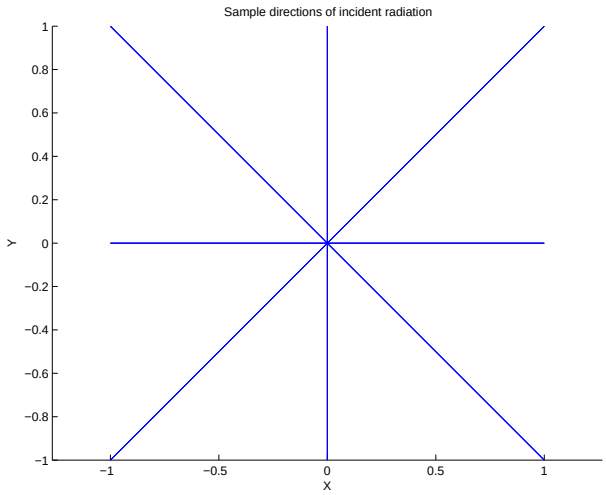


Figure 12: Sample directions/Z View

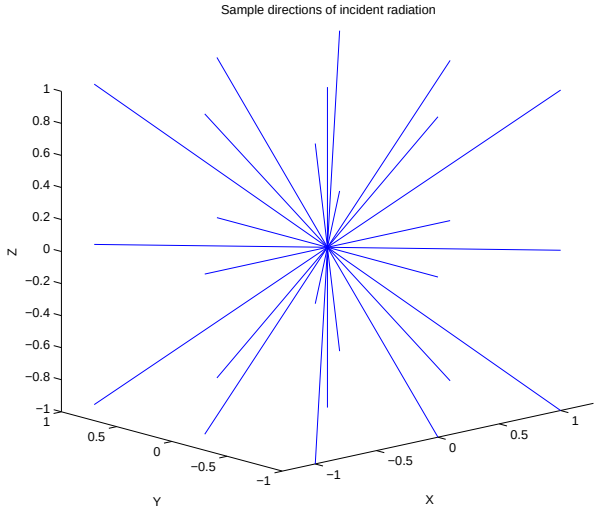


Figure 13: Sample directions/Oblique View

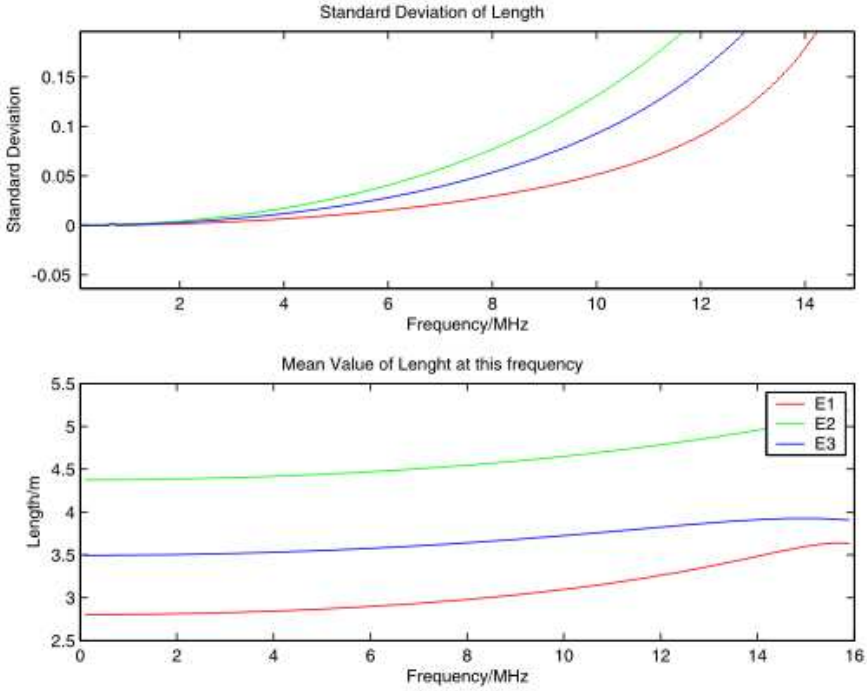


Figure 14: Standard deviation of the length

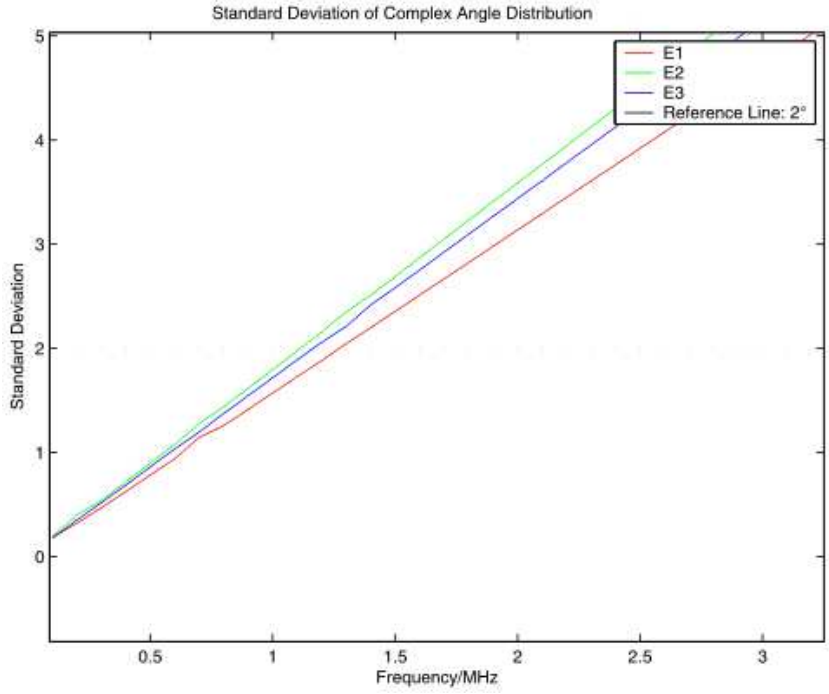


Figure 15: Complex standard deviation of the angular distribution

and

$$10^{-6} \cdot \begin{pmatrix} \mathbf{1.372} & -1.006 & -1.391 & -11.33 & 1.601 & -10.15 & -5.981 & -2.448 & -.8297 \\ -1.006 & \mathbf{8.824} & -1.152 & 9.413 & -13.79 & -7.628 & 7.825 & 11.31 & 3.455 \\ -1.391 & -1.152 & \mathbf{3.985} & 11.97 & 1.095 & 27.79 & 4.510 & -.6209 & -.5911 \\ -11.33 & 9.413 & 11.97 & \mathbf{98.07} & -15.91 & 84.51 & 54.02 & 23.15 & 10.93 \\ 1.601 & -13.79 & 1.095 & -15.90 & \mathbf{21.90} & 7.589 & -12.90 & -17.84 & -5.881 \\ -10.15 & -7.628 & 27.79 & 84.51 & 7.589 & \mathbf{195.9} & 30.75 & -4.497 & -6.235 \\ -5.981 & 7.824 & 4.510 & 54.01 & -12.90 & 30.75 & \mathbf{32.59} & 16.93 & 9.417 \\ -2.449 & 11.30 & -.6209 & 23.15 & -17.83 & -4.498 & 16.93 & \mathbf{16.58} & 6.860 \\ -.8297 & 3.455 & -.5911 & 10.94 & -5.882 & -6.235 & 9.417 & 6.860 & \mathbf{5.692} \end{pmatrix} \quad (4)$$

The variances and covariances are rather small at low frequencies. Further research shows that they suddenly explode at about 12MHz. At 16MHz the variances of the angles have an order of magnitude of 30-40 degrees.

## 3.3 Variation of the effective length vectors with frequency at fixed direction

The radiation, the spacecraft will measure, will arrive roughly from the sun, which is located opposite to the boom (positive x-axis). Therefore, like in the first report, we present in detail the response of the antennas to waves incident from the positive x-direction. (Fig. 16- 18)

The resonance is not visible, anymore. One possible explanation could be that, due to the configuration change, the first resonance would occur at a higher frequency than 16MHz. Since the boom is now nearer to the antennas than at the first models, this would seem logical.

## 3.4 Variation of the effective length vectors with different HGA angles

Similar to the visualization of the dependence of the effective length vectors on the direction of the radiation, their dependence on the position of the HGA dish can be shown. Like before, the frequency is color coded.

Figures 19-21 show the result in graphical form, while table 3-5 show the numerical values for a frequency of 500kHz. The distribution seems to be not as spread as in the case of the different incident directions, but it is, never the less, clearly visible at high frequencies.

Table 3: Variation of E1 due to HGA angle variation

| HGA angle | $\sigma_{h_{eff}}$ | $\sigma_\zeta$ | $\sigma_\xi$ |
|---|---|---|---|
| -90 | 2.82 | 136.3 | 19.6 |
| -80 | 2.82 | 136.3 | 19.5 |
| -70 | 2.82 | 136.2 | 19.5 |
| -60 | 2.82 | 136.1 | 19.5 |
| -50 | 2.82 | 136.1 | 19.5 |
| -40 | 2.82 | 136.1 | 19.5 |
| -30 | 2.81 | 136.2 | 19.2 |
| -20 | 2.81 | 135.9 | 19.8 |
| -10 | 2.81 | 135.9 | 20.0 |
| 0 | 2.80 | 135.8 | 20.2 |
| 10 | 2.81 | 135.6 | 20.2 |
| 20 | 2.81 | 135.3 | 20.2 |
| 30 | 2.81 | 135.1 | 20.3 |
| 40 | 2.81 | 134.9 | 20.3 |
| 50 | 2.81 | 134.7 | 20.4 |
| 60 | 2.80 | 134.6 | 20.5 |
| 70 | 2.80 | 134.6 | 20.5 |
| 80 | 2.80 | 134.7 | 20.6 |
| 90 | 2.79 | 134.8 | 20.7 |

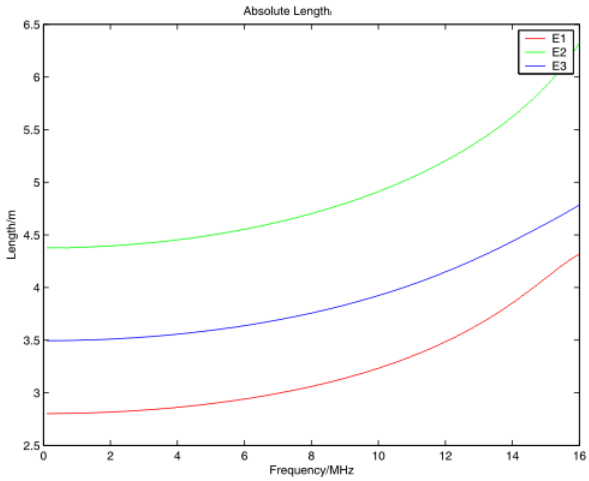


Figure 16: The absolute values of the coordinates of the electric antennas of the design 1 model.

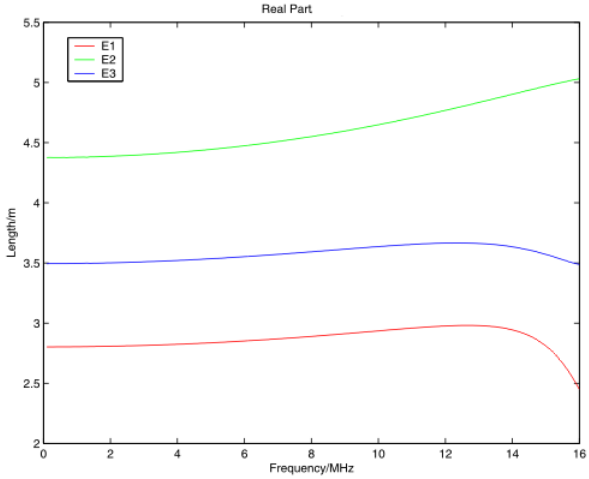


Figure 17: The real parts of the coordinates of the electric antennas of the design 1 model.

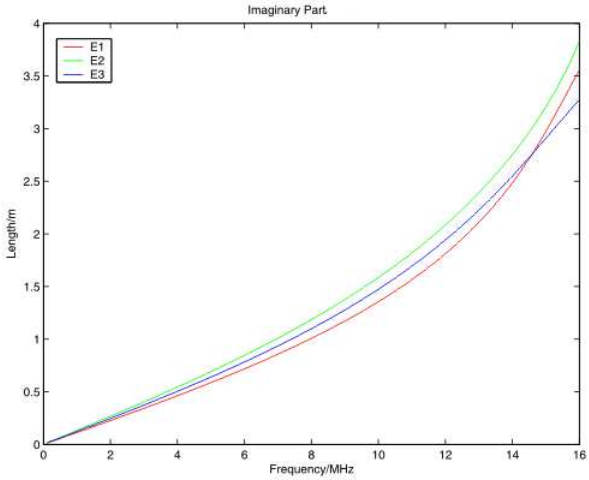




Figure 18: The imaginary parts of the coordinates of the electric antennas of the design 1 model.

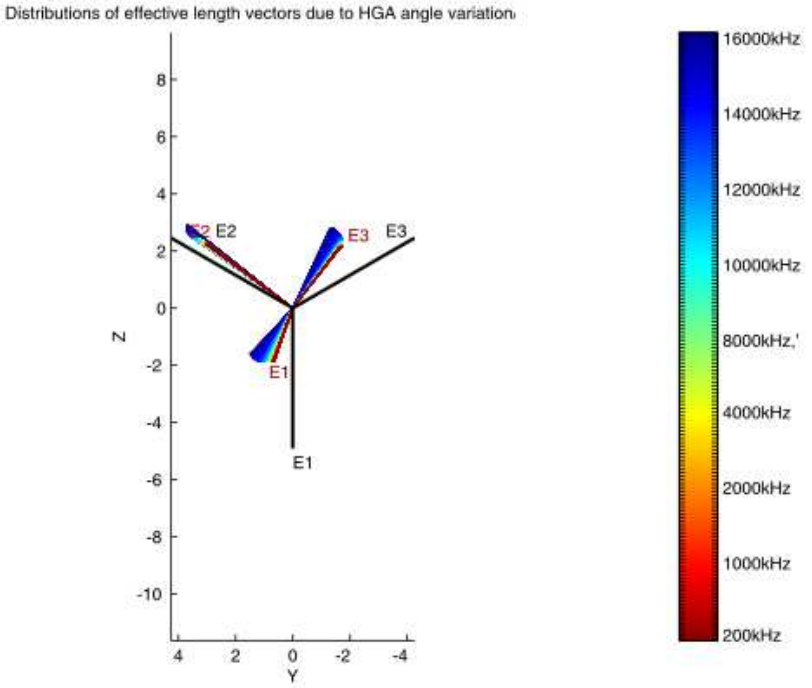


Figure 19: The spatial distribution of the real parts of the effective length vectors of the design 1 model/X View

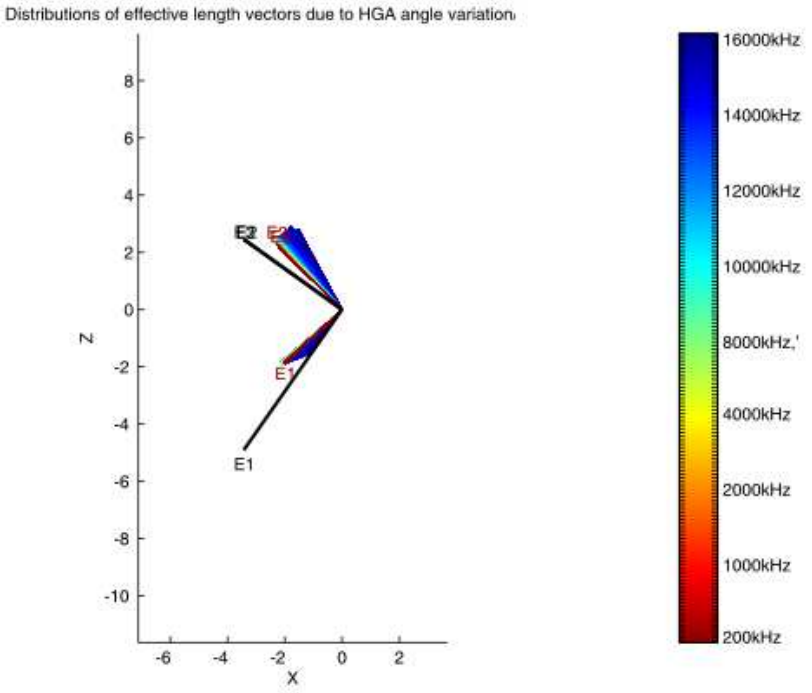


Figure 20: The spatial distribution of the real parts of the effective length vectors of the design 1 model/Y View

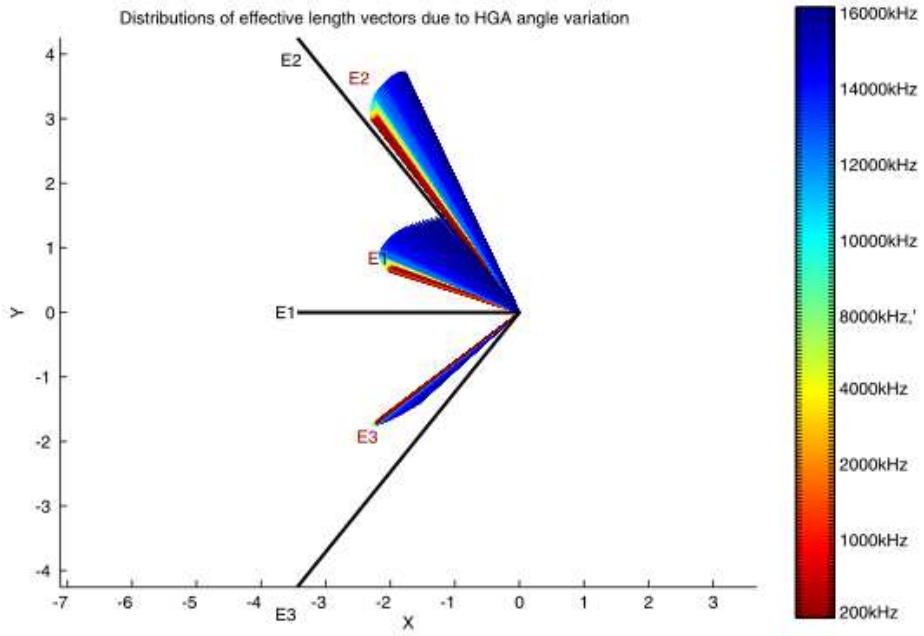


Figure 21: The spatial distribution of the real parts of the effective length vectors of the design 1 model/Z View

Table 4: Variation of E2 due to HGA angle variation

| HGA angle | $\sigma_{h_{eff}}$ | $\sigma_\zeta$ | $\sigma_\xi$ |
|---|---|---|---|
| -90 | 4.38 | 121.5 | 127.3 |
| -80 | 4.37 | 121.5 | 127.3 |
| -70 | 4.37 | 121.5 | 127.2 |
| -60 | 4.37 | 121.5 | 127.2 |
| -50 | 4.37 | 121.5 | 127.1 |
| -40 | 4.37 | 121.4 | 127.2 |
| -30 | 4.36 | 121.5 | 127.4 |
| -20 | 4.37 | 121.3 | 127.1 |
| -10 | 4.37 | 121.2 | 127.1 |
| 0 | 4.38 | 121.1 | 127.1 |
| 10 | 4.37 | 121.0 | 126.9 |
| 20 | 4.36 | 120.9 | 126.7 |
| 30 | 4.36 | 120.8 | 126.6 |
| 40 | 4.35 | 120.7 | 126.4 |
| 50 | 4.35 | 120.6 | 126.3 |
| 60 | 4.35 | 120.6 | 126.3 |
| 70 | 4.35 | 120.6 | 126.3 |
| 80 | 4.36 | 120.7 | 126.4 |
| 90 | 4.36 | 120.6 | 126.6 |

Table 5: Variation of E3 due to HGA angle variation

| HGA angle | $\sigma_{h_{eff}}$ | $\sigma_\zeta$ | $\sigma_\xi$ |
|---|---|---|---|
| -90 | 3.54 | 129.1 | -142.0 |
| -80 | 3.54 | 129.1 | -141.9 |
| -70 | 3.53 | 129.1 | -141.9 |
| -60 | 3.52 | 129.1 | -141.9 |
| -50 | 3.52 | 129.1 | -141.9 |
| -40 | 3.52 | 129.1 | -142.0 |
| -30 | 3.53 | 129.0 | -141.7 |
| -20 | 3.50 | 129.0 | -142.2 |
| -10 | 3.50 | 129.0 | -142.4 |
| 0 | 3.50 | 128.8 | -142.6 |
| 10 | 3.47 | 128.8 | -142.6 |
| 20 | 3.44 | 128.8 | -142.6 |
| 30 | 3.40 | 128.8 | -142.6 |
| 40 | 3.37 | 128.8 | -142.6 |
| 50 | 3.35 | 128.8 | -142.7 |
| 60 | 3.34 | 128.7 | -142.7 |
| 70 | 3.35 | 128.6 | -142.8 |
| 80 | 3.37 | 128.6 | -142.9 |
| 90 | 3.39 | 128.5 | -124.0 |

As before the use of the virtual Macher Angle can be used to quantify the situation. (Figures 22 and 23) In figure 23 one can see that the variation of the direction of the effective height vector for E3 is larger then for the other antennas. The reason is that E3 is located nearest to the HGA dish, so the influence of its location and direction is highest in this antenna.

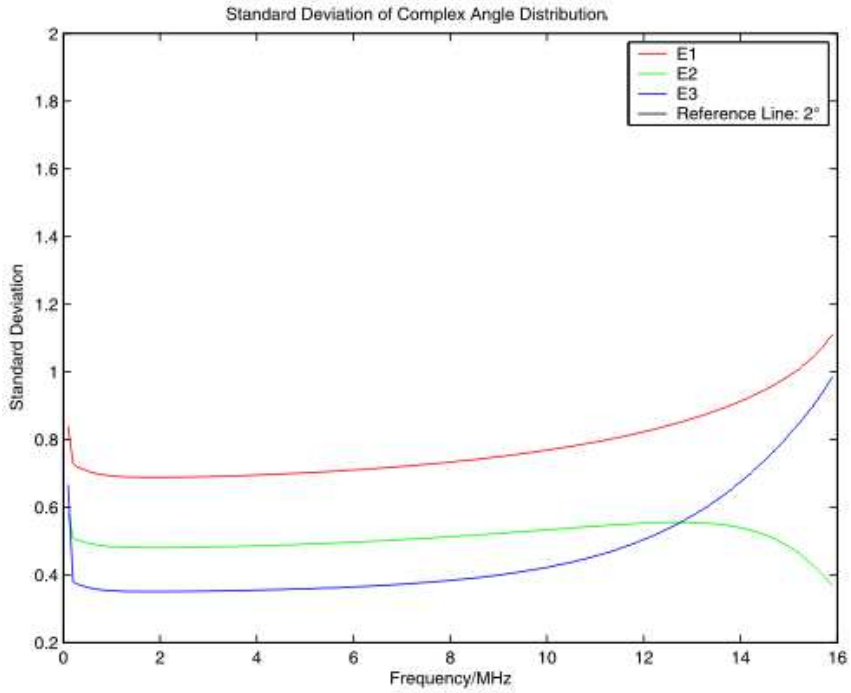


Figure 22: Complex standard deviation of the angular distribution due to HGA angle variation

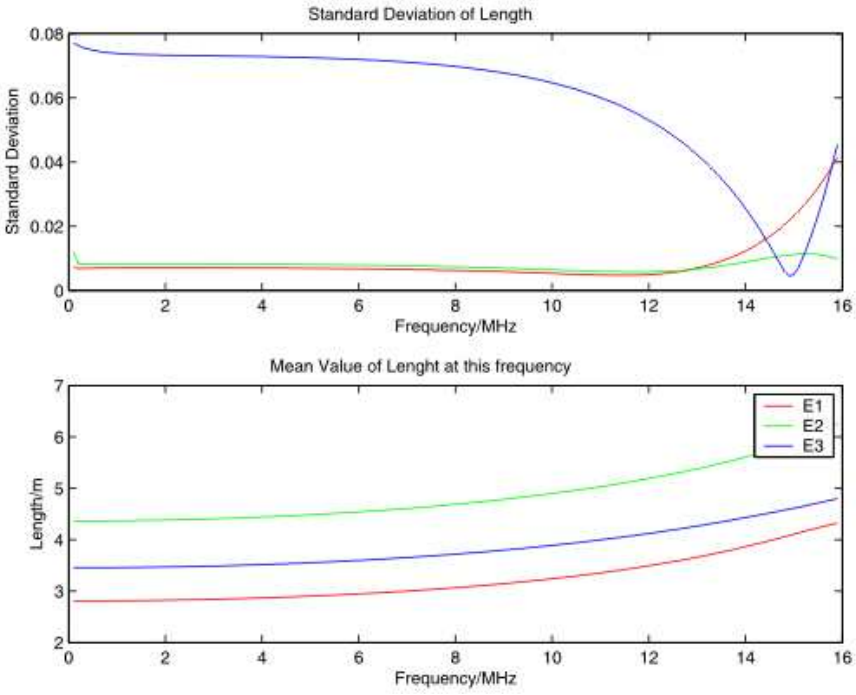


Figure 23: Standard deviation of the length due to HGA angle variation

### 3.5 The impedances and admittances

The Impedances and Admittances of the three antennas as a function of frequency are shown in Figures 24 to 27.

The first resonances occur at the same frequency as at the previous model.

## 4 Calculations, with base capacitances included

The next step is to include the capacitances as in tabulated table 1. We did perform all computations again, and studied the differences to the first results to find out how significant the influence of the capacitances is. The capacitance of the receiver is not known, but estimated on base of our experience from Cassini. The capacitances are included as impedances when calculating the transfer matrices.

Figures 28-30 show plots of the resultant effective axis. The frequency used for these plots is, again, 500kHz, and the direction of the incident wave is from the positive x-axis.

The following table shows the directions and lengths of the electric and physical antennas at a frequency of 500kHz. The direction to the origin of the wave is, again, the positive x-axis. For comparison, the values calculated without considering the influence of the capacitances is included (from table 2).

Table 6: Effective length vectors at 500kHz with capacitances included

| | | Without Capacitances | With Capacitances | Physical antennas |
|---|---|---|---|---|
| E1 | Length/m | 2.80 | 0.83 | 6.00 |
| | $\zeta/°$ | 135.5 | 128.3 | 125.26 |
| | $\xi/°$ | 20.1 | 15.0 | 0.0 |
| E2 | Length/m | 4.38 | 1.21 | 6.00 |
| | $\zeta/°$ | 120.9 | 117.1 | 125.26 |
| | $\xi/°$ | 127.1 | 125.8 | 120.0 |
| E3 | Length/m | 3.49 | 0.99 | 6.00m |
| | $\zeta/°$ | 128.5 | 123.5 | 125.26 |
| | $\xi/°$ | -142.5 | -137.2 | -120.0 |

According to this table, the influence of the capacitances on the effective length vectors seem to be substantial.

### 4.1 Variation of the effective length vectors with frequency and direction

Plot 31 was generated in the same way as without capacitances, nevertheless, the difference is not hard to spot. The reason for this erratic behavior is that the resonance was shifted below 16MHz as a result of the inclusion of the capacitances. For comparison, figures 32 and 32 show a plot, generated the same way, but with a frequency range up to only 13MHz and 12MHz, respectively.

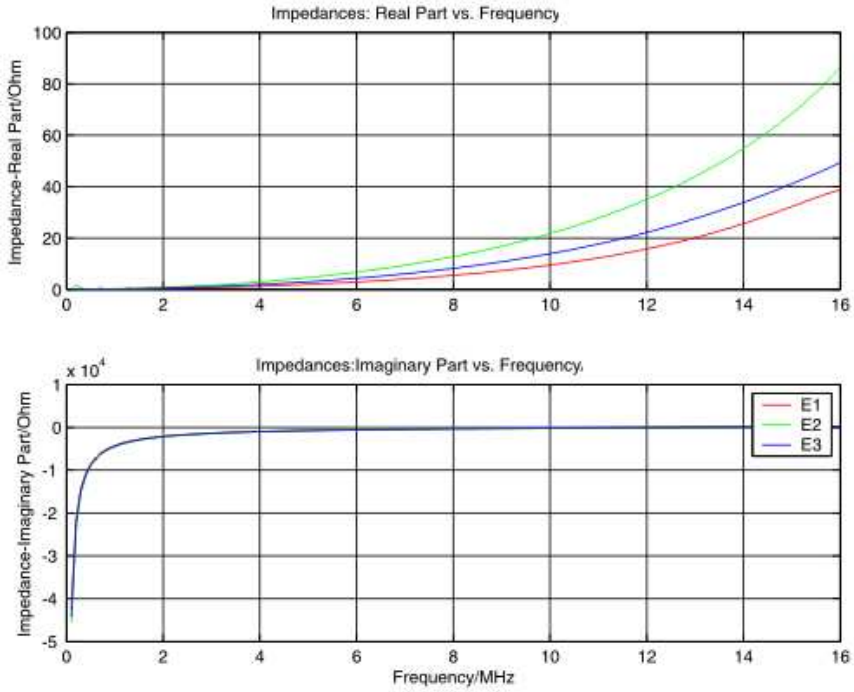


Figure 24: Impedances of Design 1

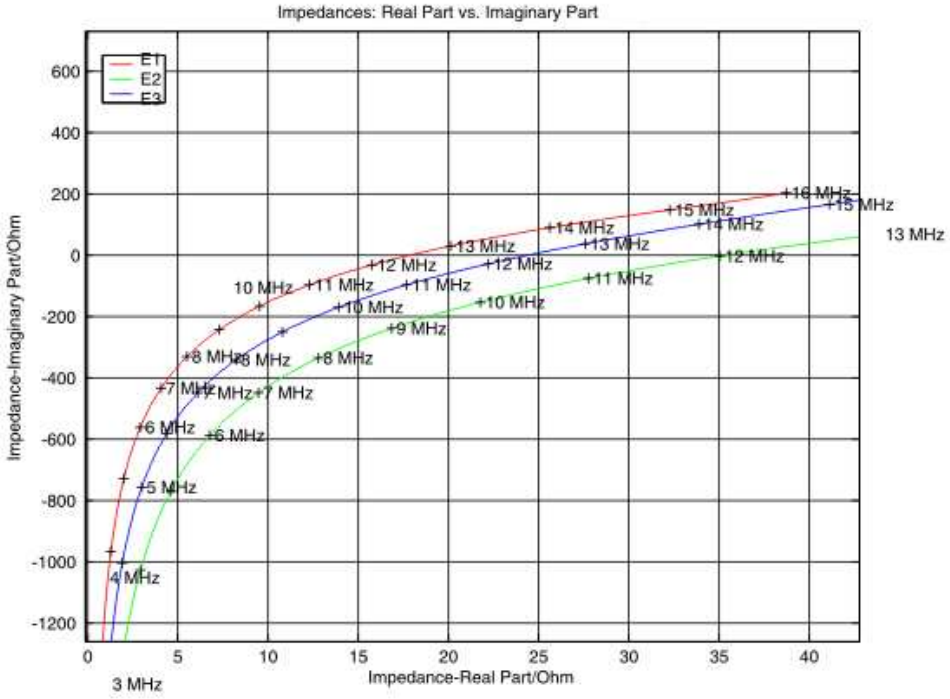


Figure 25: Impedances of Design 1

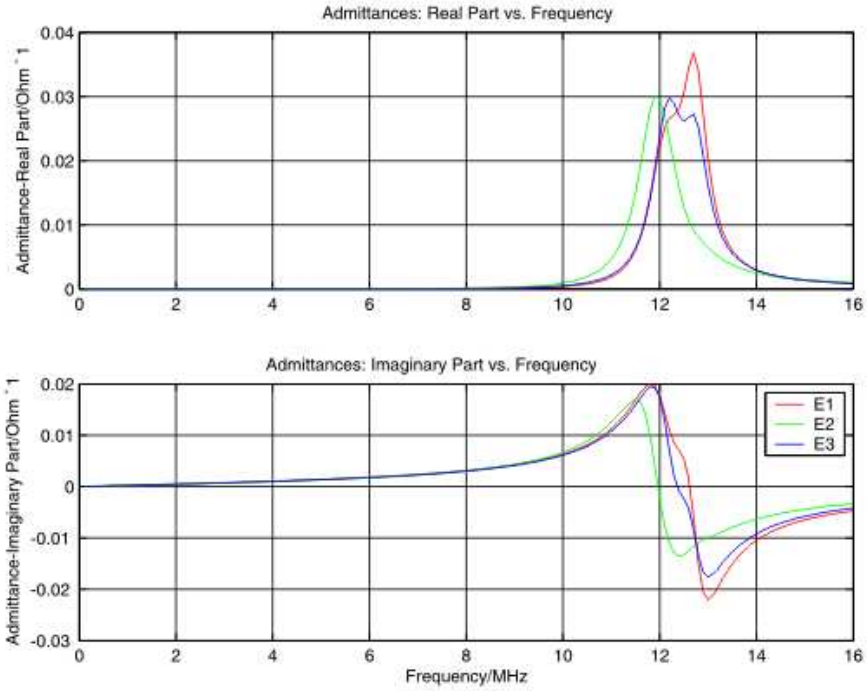


Figure 26: Admittances of Design 1

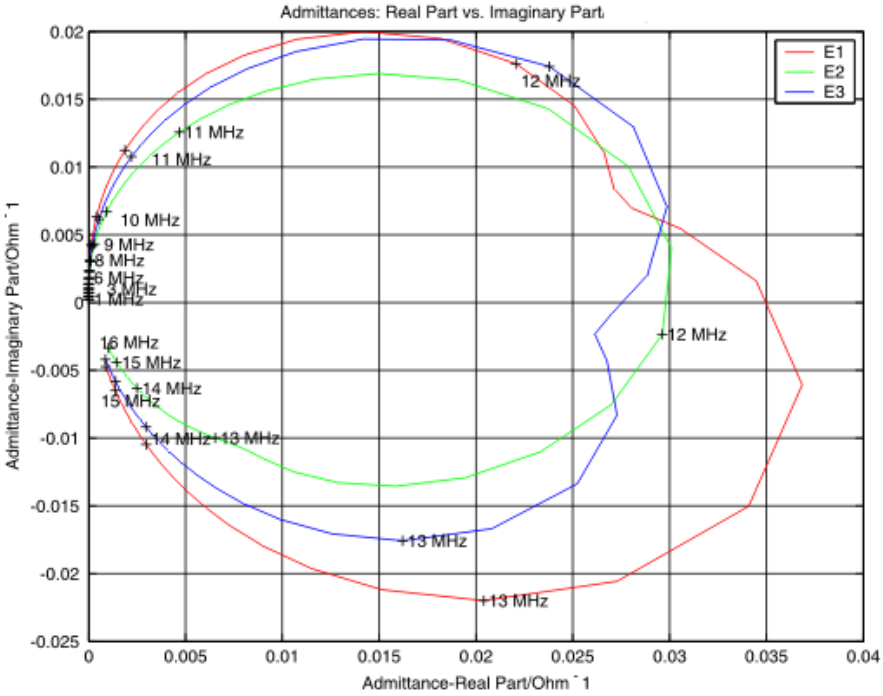


Figure 27: Admittances of Design 1

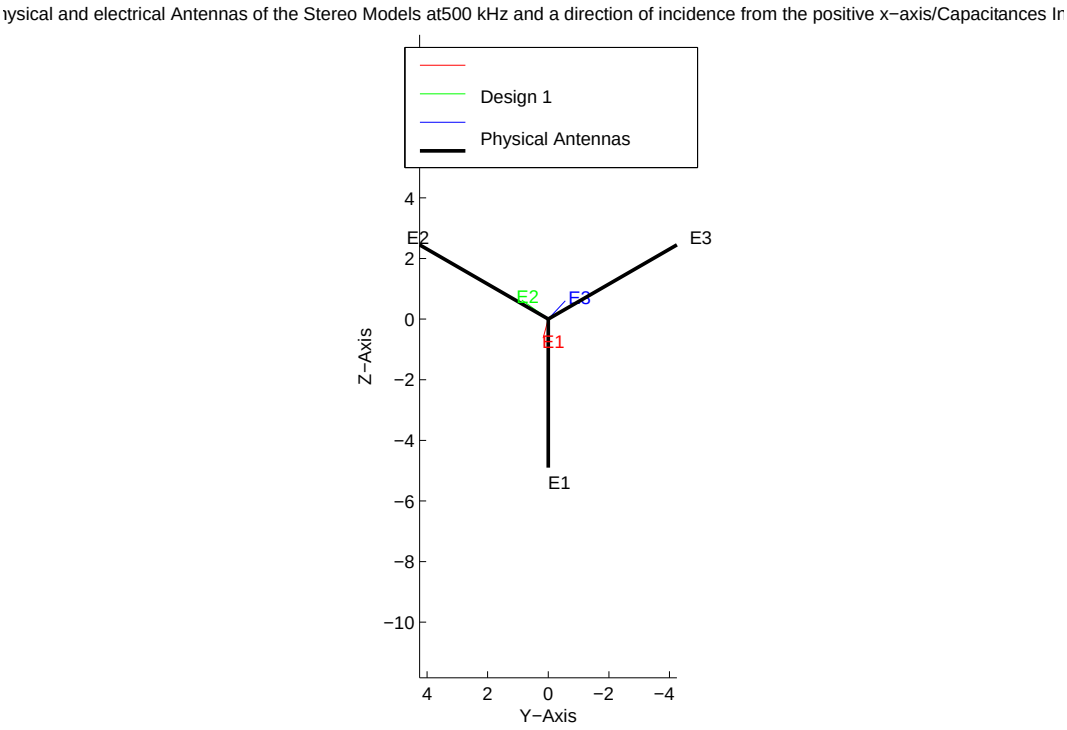


Figure 28: Spacecraft A: Effective Length Vectors,X-View/ Capacitances included

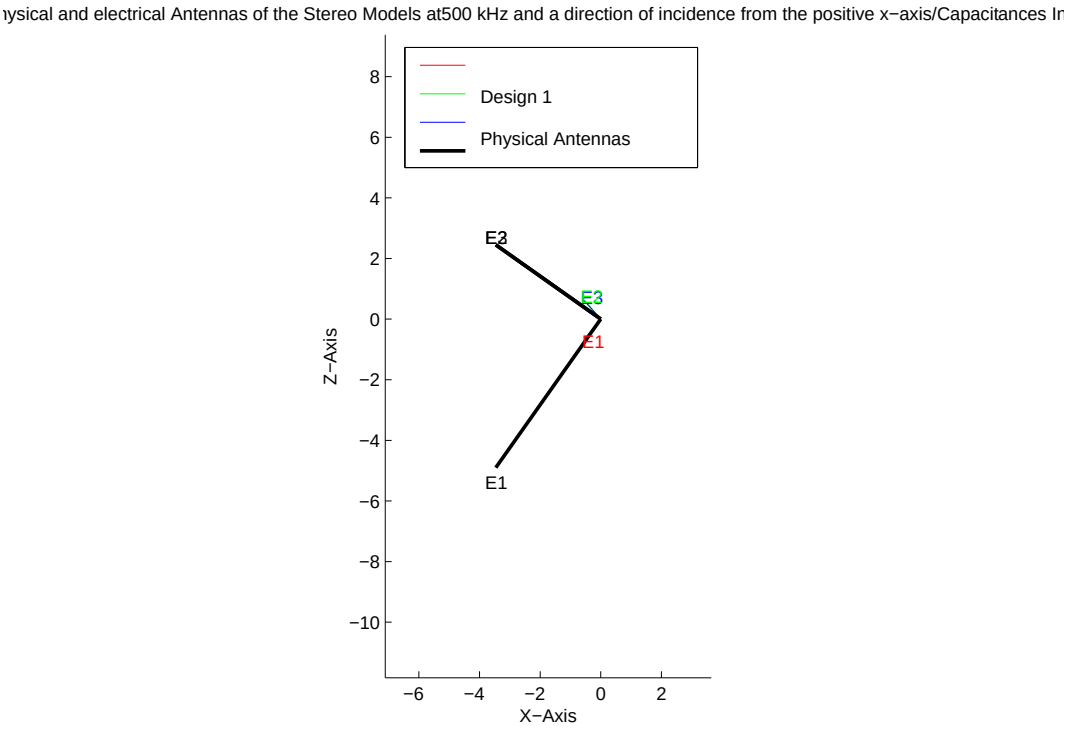


Figure 29: Spacecraft A: Effective Length Vectors,Y-View/ Capacitances included

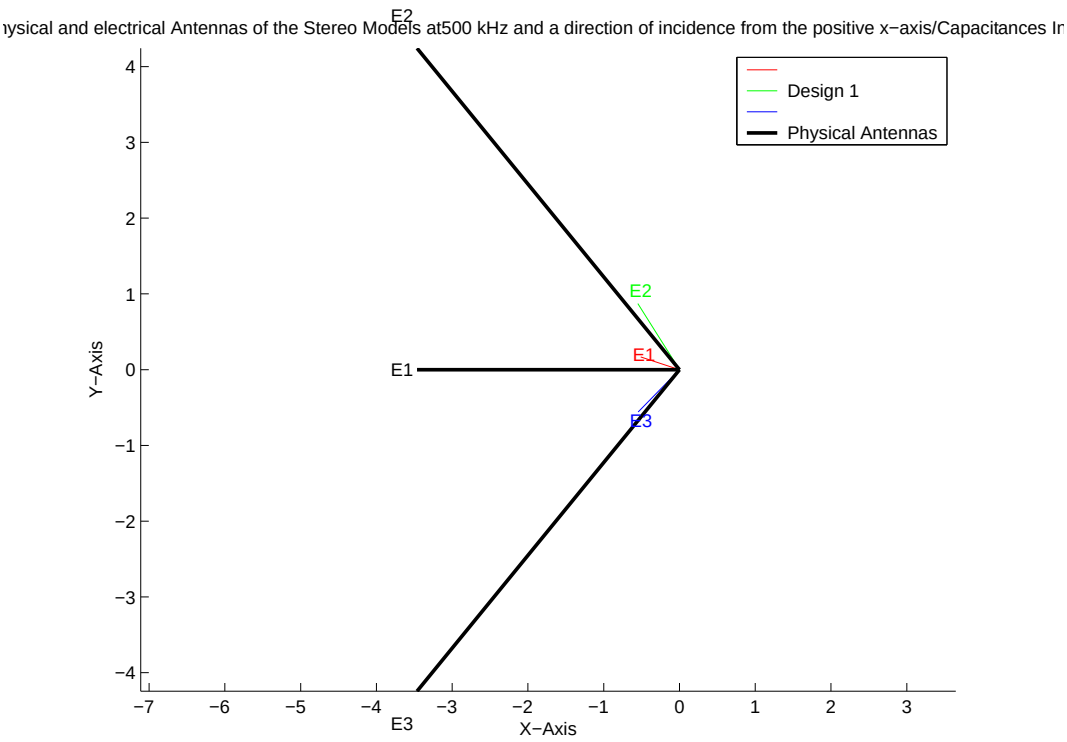


Figure 30: Spacecraft A: Effective Length Vectors,Z-View/ Capacitances included

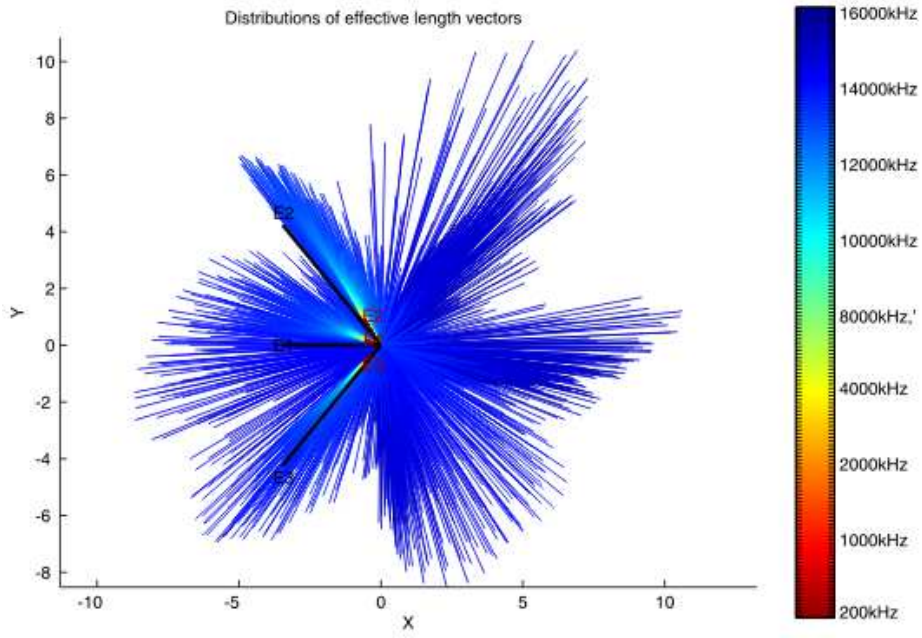


Figure 31: The spatial distribution of the real parts of the effective length vectors of the design 1 model with capacitances included-16MHz/Z View

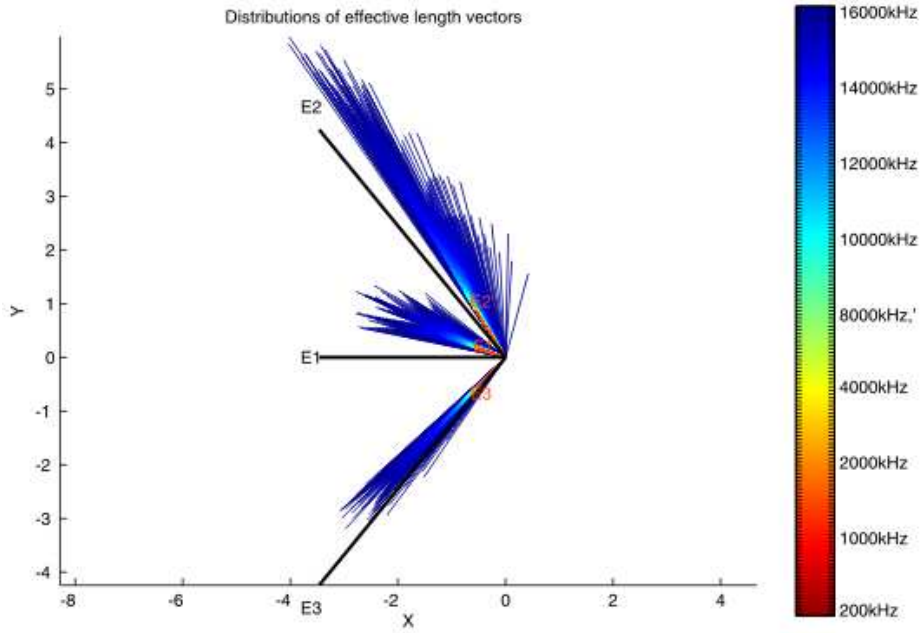


Figure 32: The spatial distribution of the real parts of the effective length vectors of the design 1 model with capacitances included-13MHz/Z View

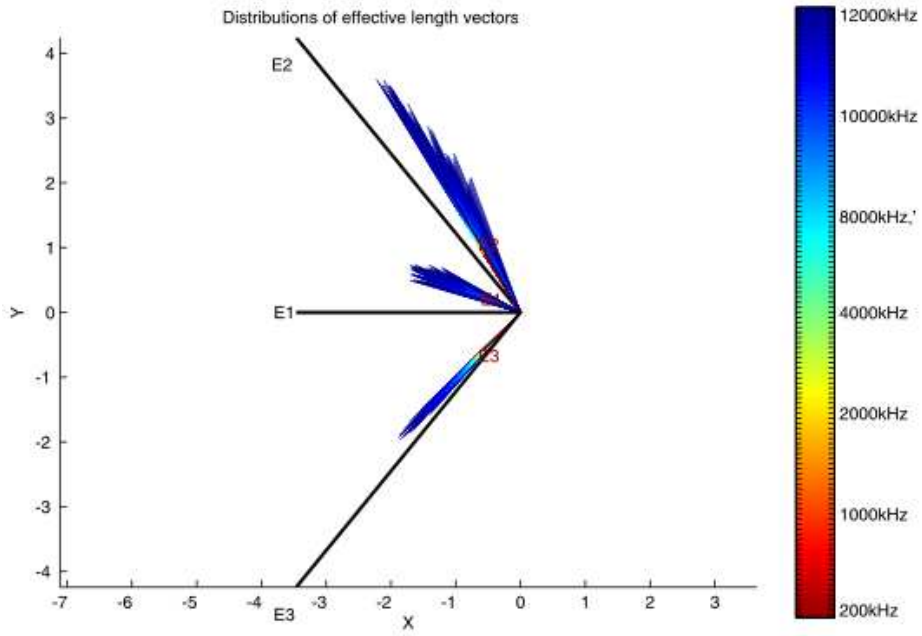


Figure 33: The spatial distribution of the real parts of the effective length vectors of the design 1 model with capacitances included-12MHz/Z View

The quantitative plots are shown in figures 34 and 35. Clearly, the resonances at 14MHz, that cause the erratic behavior regarding the direction dependency of the effective length vectors, are reflected in their standard deviations.

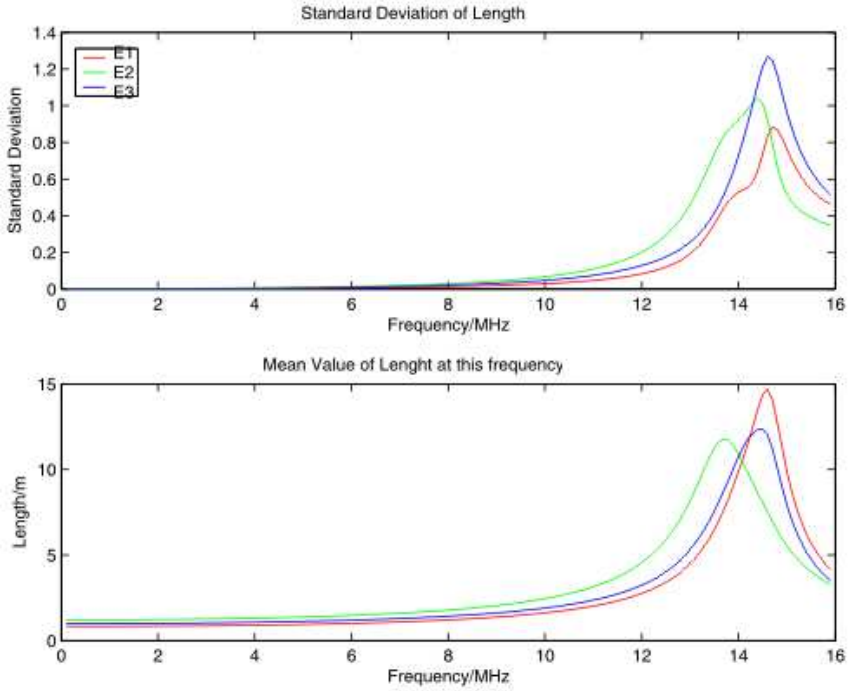


Figure 34: Standard deviation of the length/Capacitances Included

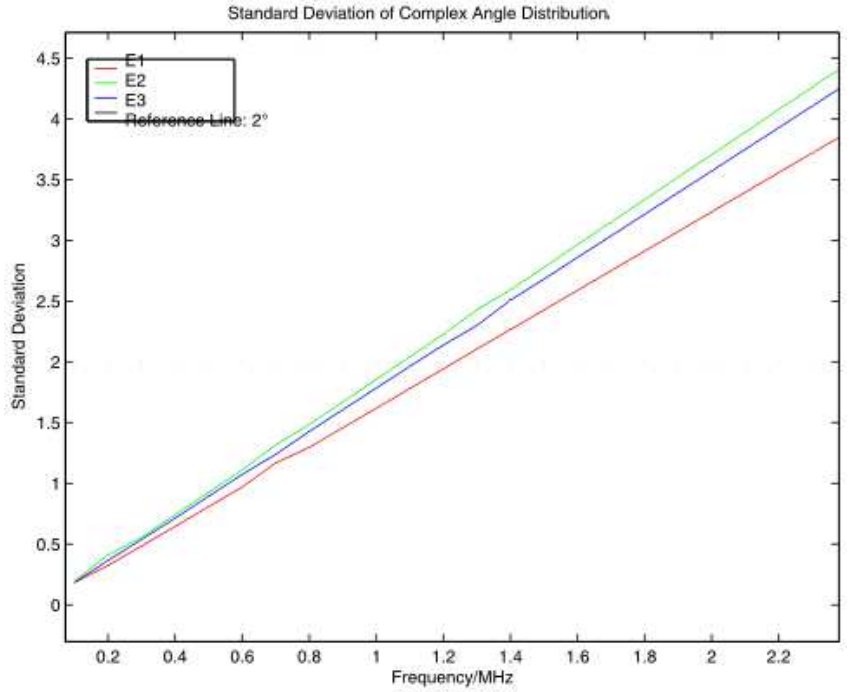


Figure 35: Complex standard deviation of the angular distribution/Capacitances included

## 4.2 The Covariance Matrix

The covariance matrices, with included capacitances at frequencies of 500kHz and 1MHz are

$$10^{-9} \cdot \begin{pmatrix} \mathbf{8.336} & -6.114 & -7.406 & -141.1 & 73.42 & -188.0 & -7.367 & -70.45 & -56.56 \\ -6.114 & \mathbf{43.39} & -6.752 & -130.5 & -186.2 & 116.8 & -17.53 & 371.1 & -74.63 \\ -7.406 & -6.752 & \mathbf{21.66} & 246.9 & -71.09 & 365.2 & -39.00 & -78.78 & 121.5 \\ -141.2 & -130.5 & 246.29 & \mathbf{4110} & -675.0 & 4056 & 207.3 & -836.4 & 1955 \\ 73.42 & -186.2 & -71.09 & -675.0 & \mathbf{1307} & -2370 & 186.3 & -1554 & -294.9 \\ -188.1 & 116.8 & 365.2 & 4056 & -2370 & \mathbf{7556} & -818.3 & 673.2 & 1835 \\ -7.367 & -17.53 & -39.00 & 207.3 & 186.3 & -818.3 & \mathbf{526.7} & 172.2 & 192.1 \\ -70.45 & 371.2 & -78.78 & -836.4 & -1554 & 673.2 & 172.2 & \mathbf{3414} & -506.3 \\ -56.56 & -74.64 & 121.5 & 1955 & -294.9 & 1835 & 192.1 & -506.3 & \mathbf{1063} \end{pmatrix} \quad (5)$$

and

$$10^{-7} \cdot \begin{pmatrix} \mathbf{1.343} & -.9867 & -1.192 & -22.50 & 11.93 & -30.54 & -1.020 & -11.42 & -8.983 \\ -.9867 & \mathbf{6.982} & -1.083 & -21.21 & -30.34 & 18.95 & -2.907 & 59.78 & -12.36 \\ -1.192 & -1.083 & \mathbf{3.491} & 39.44 & -11.57 & 59.07 & -6.382 & -12.51 & 19.55 \\ -22.50 & -21.21 & 39.44 & \mathbf{655.9} & -107.5 & 649.7 & 32.04 & -135.2 & 314.8 \\ 11.93 & -30.34 & -11.57 & -107.5 & \mathbf{214.7} & -387.0 & 31.61 & -253.8 & -45.59 \\ -30.53 & 18.95 & 59.07 & 649.7 & -387.0 & \mathbf{1230} & -137.3 & 112.2 & 292.5 \\ -1.020 & -2.907 & -6.382 & 32.04 & 31.61 & -137.3 & \mathbf{84.54} & 25.64 & 31.20 \\ -11.42 & 59.78 & -12.51 & -135.7 & -253.8 & 112.2 & 25.64 & \mathbf{549.4} & -84.16 \\ -8.983 & -12.36 & 19.55 & 314.8 & -45.59 & 292.5 & 31.20 & -84.16 & \mathbf{171.6} \end{pmatrix} \quad (6)$$

The order of the parameters is $h_{eff}(E1), h_{eff}(E2), h_{eff}(E3), \phi(E1), \phi(E2), \phi(E3), \theta(E1), \theta(E2), \theta(E3)$, as before. The variances and covariances seem to be smaller, when the capacitances are included in the calculation.

## 4.3 Variation of the effective length vectors with frequency at fixed direction

The response of the antennas to waves incident from the positive x-direction. (fig. 36 - 38)

Contrary to the result without capacitances, the resonance is clearly visible.

## 4.4 Variation of the effective length vectors with different HGA angles

Figures 40-39 show the color coded plots that show the variability of the electric antennas due to the turnable HGA dish. Figure 39 shows the same scenario as with the different directions of incidence. Also the different angles of the HGA dish has a great influence upon the receiving properties of the stacer antennas at a frequency of 14MHz. Figures 40-42 are created with a frequency range up to 13MHz which is short below the resonance frequency. The erratic behavior vanished.

Table 7: Variation of E1 due to HGA angle variation with base capacitances included

| HGA angle | $\sigma_{h_{eff}}$ | $\sigma_\zeta$ | $\sigma_\xi$ |
|---|---|---|---|
| -90 | 0.83 | 128.5 | 14.5 |
| -80 | 0.83 | 128.5 | 14.5 |
| -70 | 0.83 | 128.5 | 14.4 |
| -60 | 0.83 | 128.4 | 14.5 |
| -50 | 0.83 | 128.4 | 14.5 |
| -40 | 0.83 | 128.4 | 14.5 |
| -30 | 0.83 | 128.4 | 14.2 |
| -20 | 0.83 | 128.3 | 14.7 |
| -10 | 0.83 | 128.3 | 14.9 |
| 0 | 0.83 | 128.2 | 15.0 |
| 10 | 0.83 | 128.1 | 15.0 |
| 20 | 0.83 | 128.0 | 15.1 |
| 30 | 0.83 | 127.8 | 15.1 |
| 40 | 0.83 | 127.7 | 15.2 |
| 50 | 0.83 | 127.7 | 15.2 |
| 60 | 0.83 | 127.6 | 15.3 |
| 70 | 0.83 | 127.6 | 15.3 |
| 80 | 0.83 | 127.7 | 15.4 |
| 90 | 0.83 | 127.7 | 15.4 |

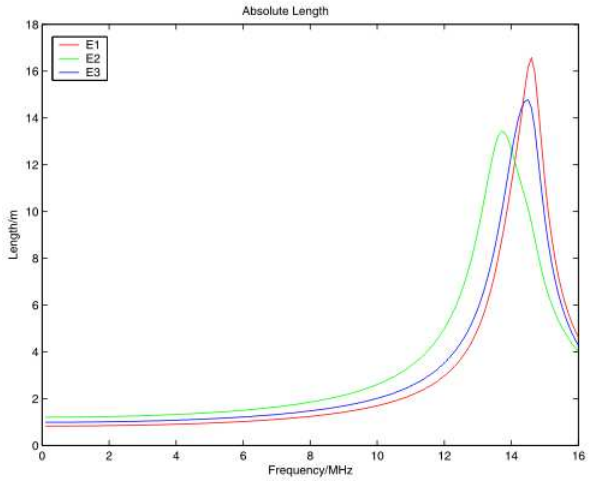


Figure 36: The absolute values of the coordinates of the electric antennas of the design 1 model/Capacitances included

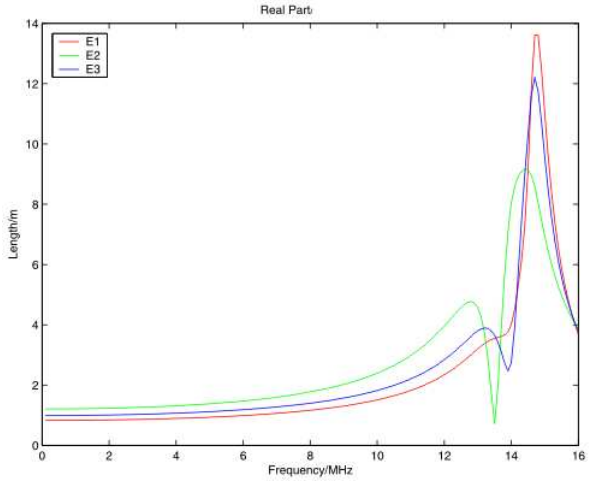


Figure 37: The real parts of the coordinates of the electric antennas of the design 1 model/Capacitances included

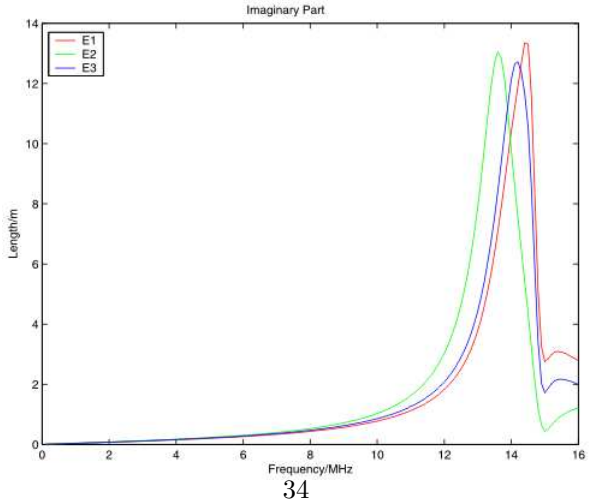




Figure 38: The imaginary parts of the coordinates of the electric antennas of the design 1 model/Capacitances included

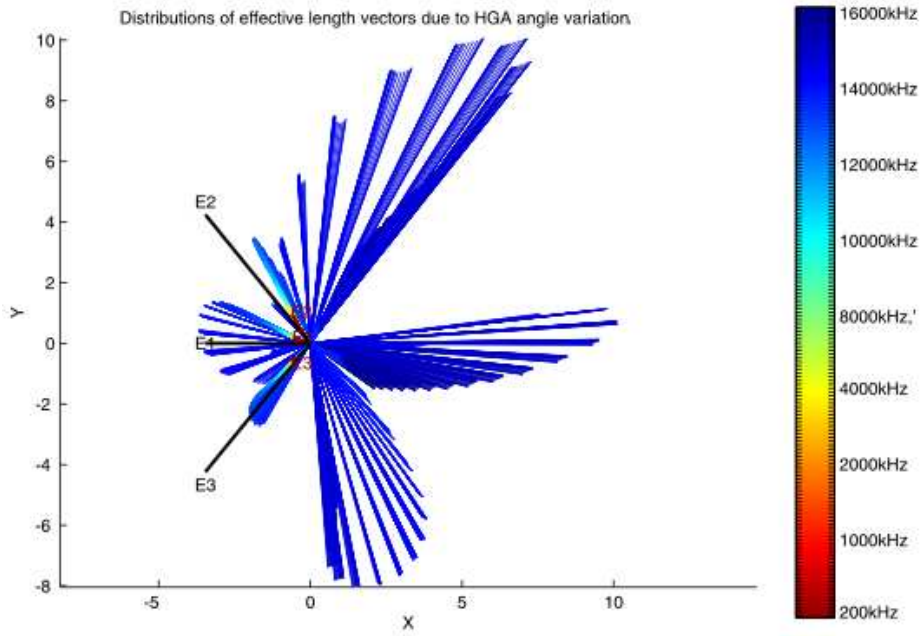


Figure 39: The spatial distribution of the real parts of the effective length vectors of the design 1 model, capacitances included/Z View

Table 8: Variation of E2 due to HGA angle variation with base capacitances included

| HGA angle | $\sigma_{h_{eff}}$ | $\sigma_\zeta$ | $\sigma_\xi$ |
|---|---|---|---|
| -90 | 1.20 | 117.4 | 125.9 |
| -80 | 1.20 | 117.4 | 125.9 |
| -70 | 1.20 | 117.4 | 125.8 |
| -60 | 1.20 | 117.4 | 125.8 |
| -50 | 1.20 | 117.3 | 125.8 |
| -40 | 1.20 | 117.3 | 125.8 |
| -30 | 1.20 | 117.3 | 125.9 |
| -20 | 1.20 | 117.2 | 125.8 |
| -10 | 1.20 | 117.2 | 125.7 |
| 0 | 1.21 | 117.1 | 125.8 |
| 10 | 1.21 | 117.0 | 125.7 |
| 20 | 1.20 | 117.0 | 125.6 |
| 30 | 1.20 | 116.9 | 125.4 |
| 40 | 1.20 | 116.9 | 125.4 |
| 50 | 1.20 | 116.8 | 125.3 |
| 60 | 1.20 | 116.8 | 125.3 |
| 70 | 1.20 | 116.8 | 125.3 |
| 80 | 1.20 | 116.8 | 125.4 |
| 90 | 1.21 | 116.8 | 125.5 |

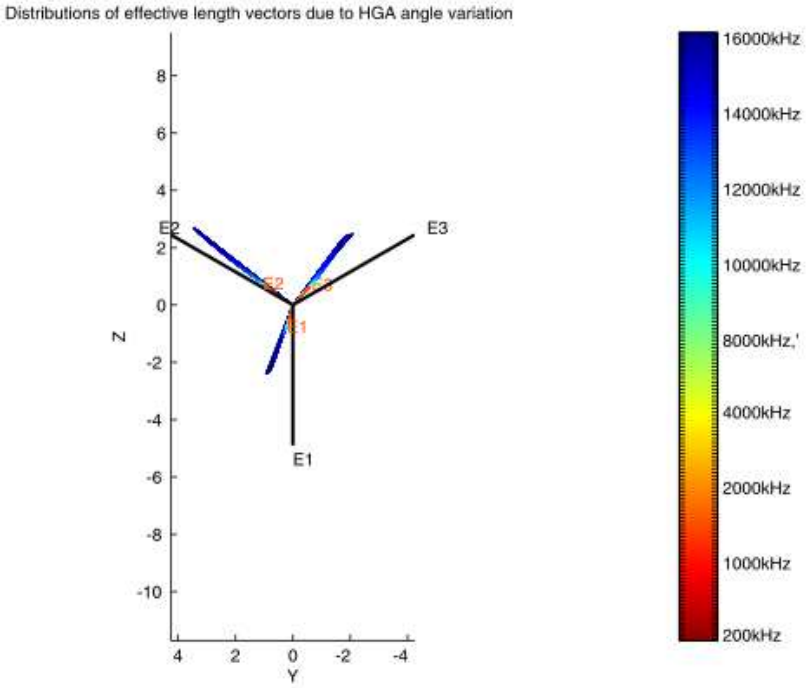


Figure 40: The spatial distribution of the real parts of the effective length vectors of the design 1 model, capacitances included/X View

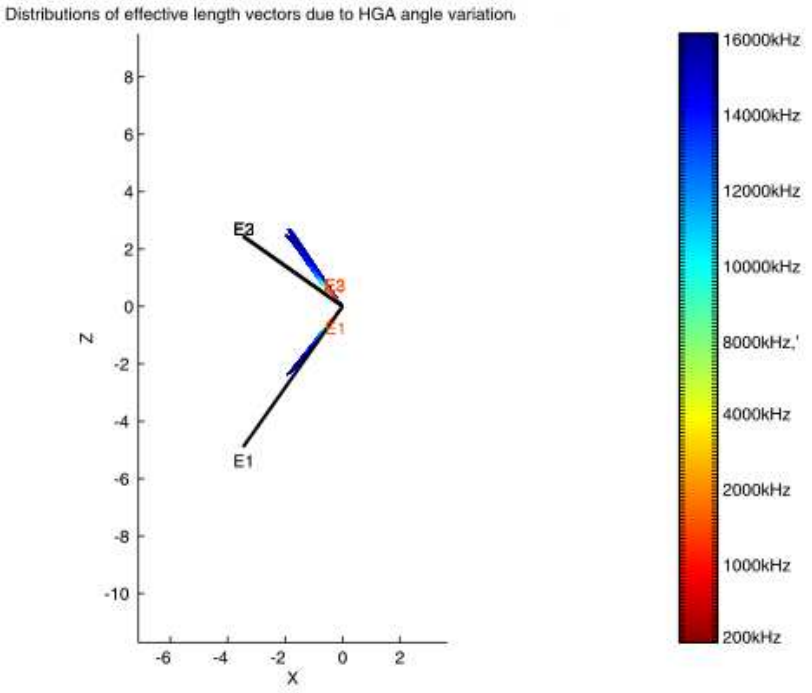


Figure 41: The spatial distribution of the real parts of the effective length vectors of the design 1 model, capacitances included/Y View

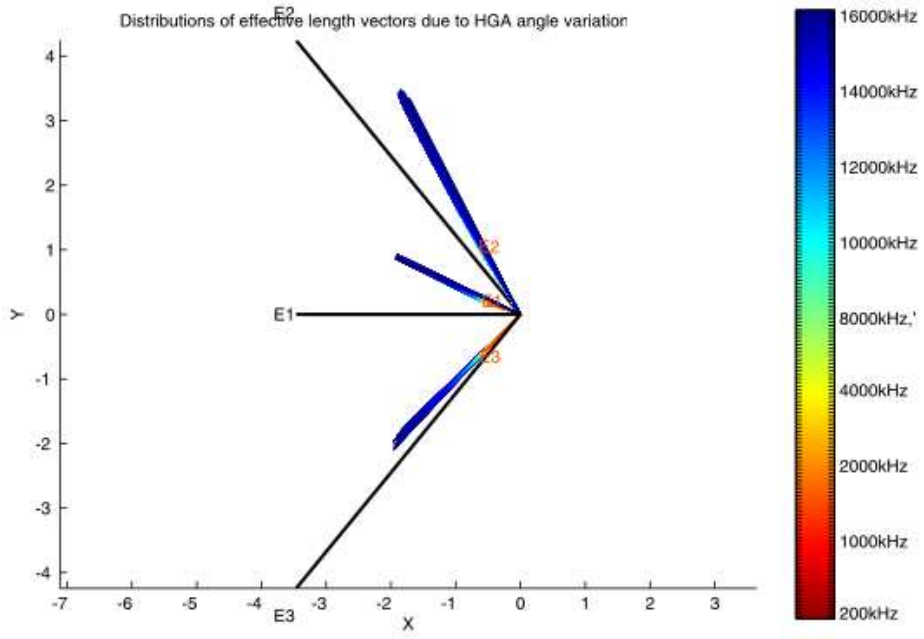


Figure 42: The spatial distribution of the real parts of the effective length vectors of the design 1 model, capacitances included/Z View

Table 9: Variation of E3 due to HGA angle variation with base capacitances included

| HGA angle | $\sigma_{h_{eff}}$ | $\sigma_\zeta$ | $\sigma_\xi$ |
|---|---|---|---|
| -90 | 1.00 | 123.7 | -136.7 |
| -80 | 1.00 | 123.7 | -136.6 |
| -70 | 0.99 | 123.7 | -136.6 |
| -60 | 0.99 | 123.7 | -136.6 |
| -50 | 0.99 | 123.7 | -136.6 |
| -40 | 0.99 | 123.7 | -136.7 |
| -30 | 0.99 | 123.4 | -136.5 |
| -20 | 0.99 | 123.6 | -136.9 |
| -10 | 0.99 | 123.6 | -137.0 |
| 0 | 0.99 | 123.5 | -137.2 |
| 10 | 0.98 | 123.5 | -137.3 |
| 20 | 0.98 | 123.5 | -137.3 |
| 30 | 0.97 | 123.6 | -137.4 |
| 40 | 0.96 | 123.6 | -137.4 |
| 50 | 0.96 | 123.6 | -137.4 |
| 60 | 0.96 | 123.5 | -137.5 |
| 70 | 0.96 | 123.5 | -137.5 |
| 80 | 0.96 | 123.4 | -137.6 |
| 90 | 0.97 | 123.3 | -137.7 |

Figures 43 and 44 show quantitatively the influence of the HGA angle.

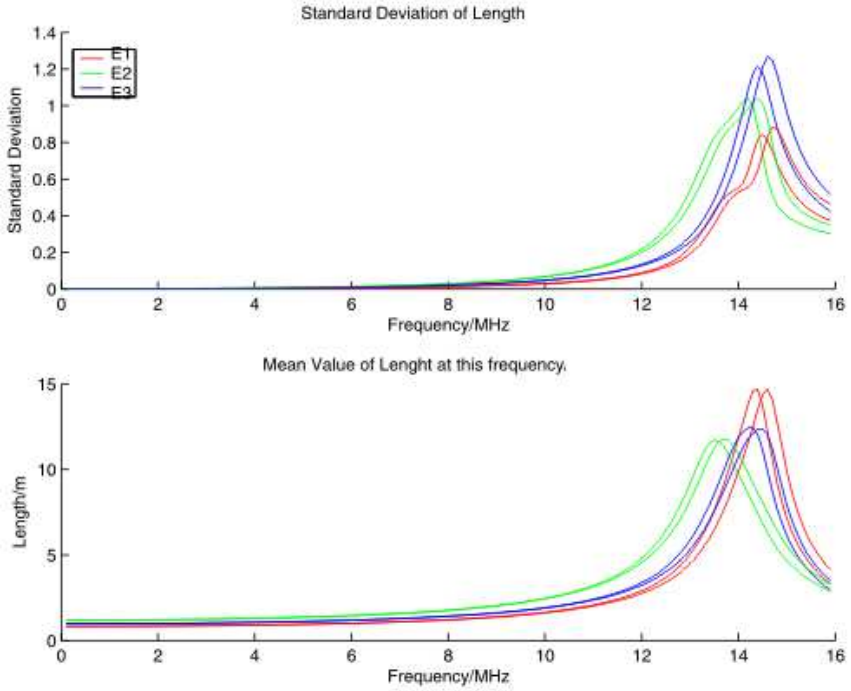


Figure 43: Complex standard deviation of the angular distribution due to HGA angle variation, capacitances included

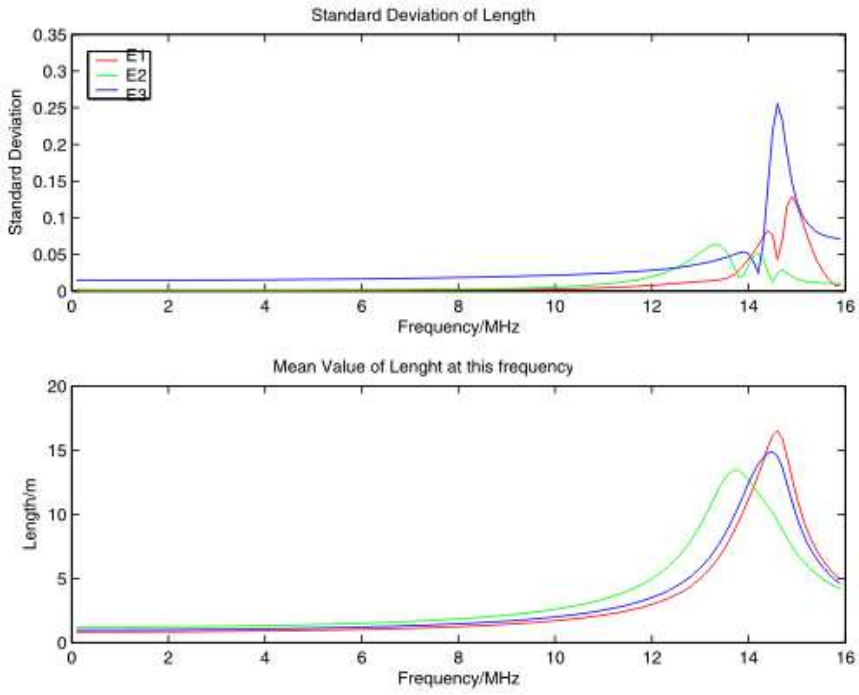


Figure 44: Standard deviation of the length due to HGA angle variation, capacitances included

## 4.5 The impedances and admittances

Since the base capacitances are parallel to the antenna capacitances, the reciprocal values have to be added to ge the total capacitance, while the admittances have simply to be added. Plots of the resultant Impedances are shown in Figures 45 and 46, plots of the resultant admittances in Figures 47 and 48.

The resonance can clearly be seen, again, at 14MHz. The inclusion of the capacitances, have the effect of increasing the imaginary part of the admittances, which, in turn, lowers the resonance frequency.

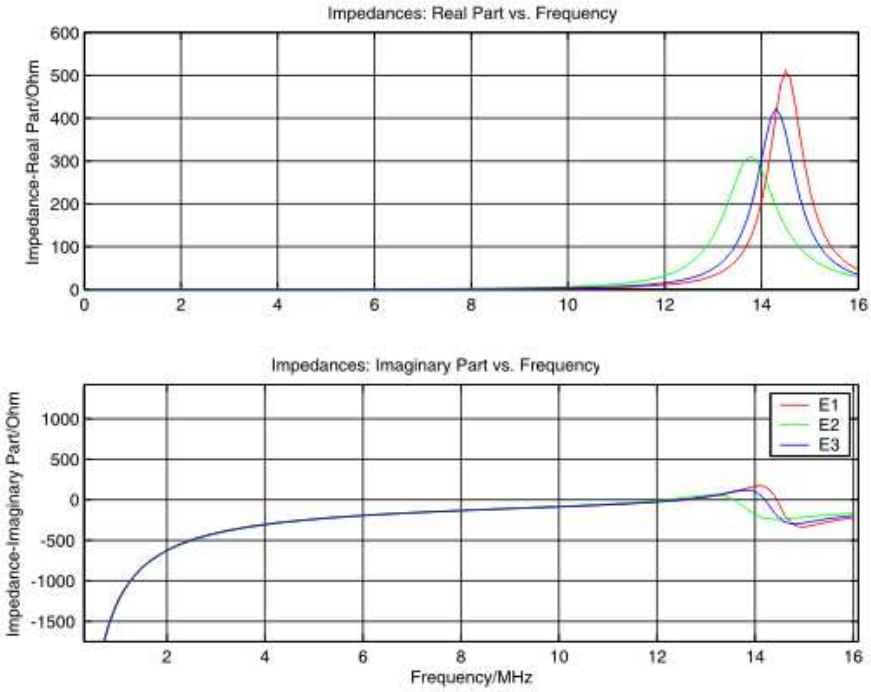


Figure 45: Impedances of Design 1, capacitances included

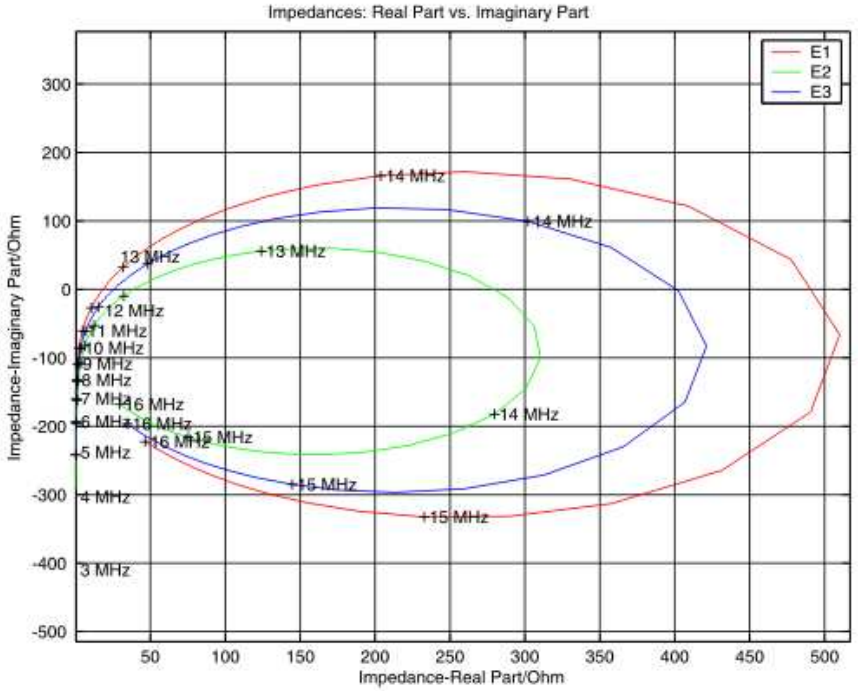


Figure 46: Impedances of Design 1, capacitances included

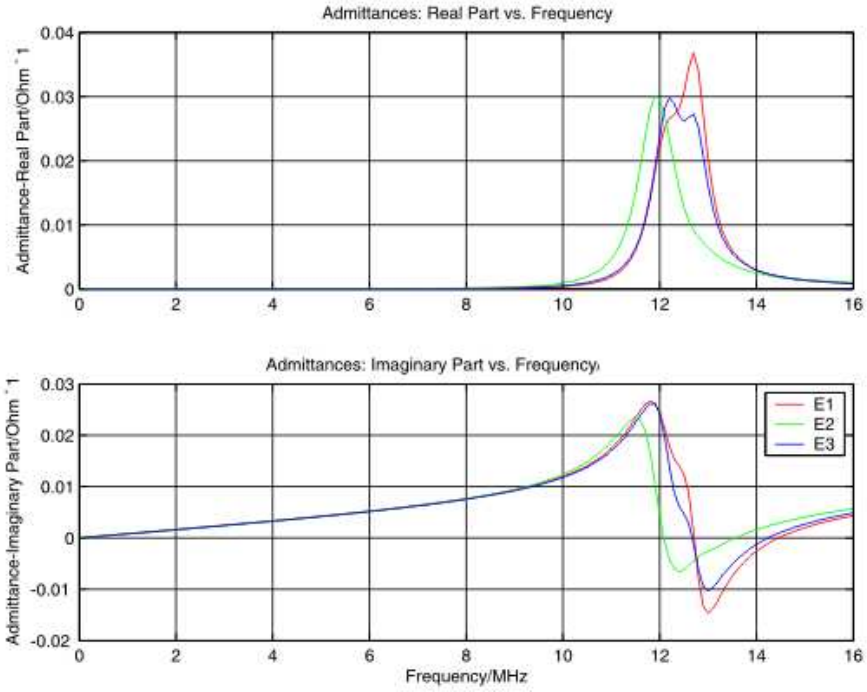


Figure 47: Admittances of Design 1, capacitances included

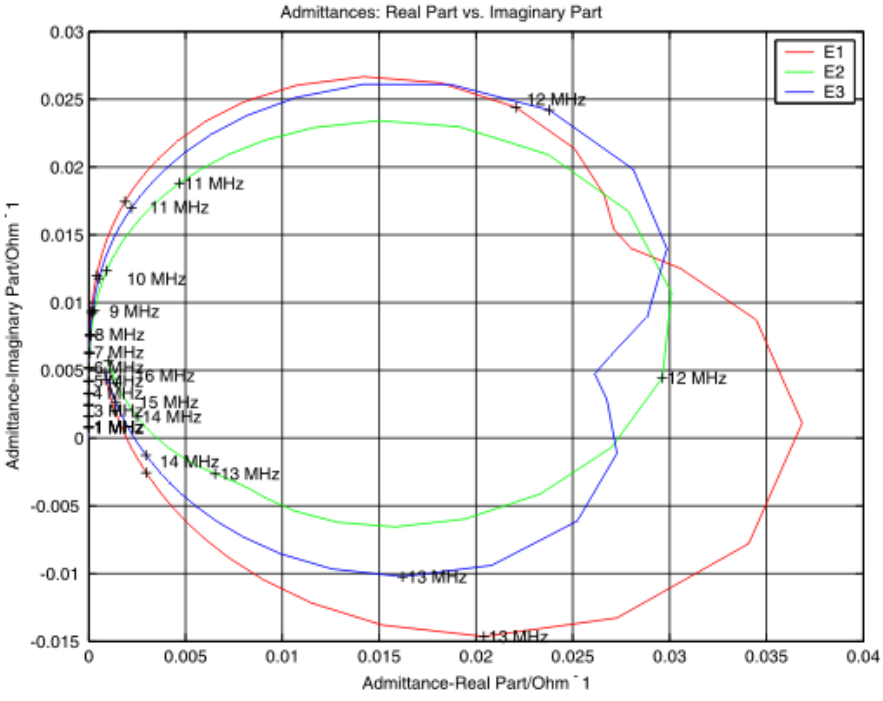


Figure 48: Admittances of Design 1, capacitances included

# Part II
# Spacecraft B

## 5 Characteristics of spacecraft B

The only difference of spacecraft B with regard to spacecraft A, that can be considered within the limitations of ASAP is the second ring which is mounted on the opposite side of the hull, directed towards the sun. (see Fig. 49)

## 6 The quasistatic regime

### 6.1 Computation of the effective length vectors

For the calculations of spacecraft B, only one angle of the HGA dish was considered.

## 7 Calculations with base capacitances included

Figures 50-52 show plots of the effective length vectors . The parameters are chosen as before.

The following table shows the directions and lengths of the electric and physical antennas at a frequency of 500kHz. For comparison, the values of spacecraft A are included.

Table 10: Effective length vectors of both spacecraft at 500kHz with capacitances included

| | | Spacecraft A | Spacecraft B | Physical antennas |
|---|---|---|---|---|
| E1 | Length/m | 0.83 | 0.84 | 6.00 |
| | $\zeta/°$ | 128.3 | 127.2 | 125.26 |
| | $\xi/°$ | 15.0 | 13.3 | 0.0 |
| E2 | Length/m | 1.21 | 1.18 | 6.00 |
| | $\zeta/°$ | 117.1 | 117.4 | 125.26 |
| | $\xi/°$ | 125.8 | 125.2 | 120.0 |
| E3 | Length/m | 0.99 | 0.98 | 6.00m |
| | $\zeta/°$ | 123.5 | 123.3 | 125.26 |
| | $\xi/°$ | -137.2 | -135.4 | -120.0 |

In the tables it can be seen, that the difference between the two spacecraft, although not large, is definitely existent.

### 7.1 Variation of the effective length vectors with frequency and direction

Plots 53-55 where generated in the same way as for spacecraft A.

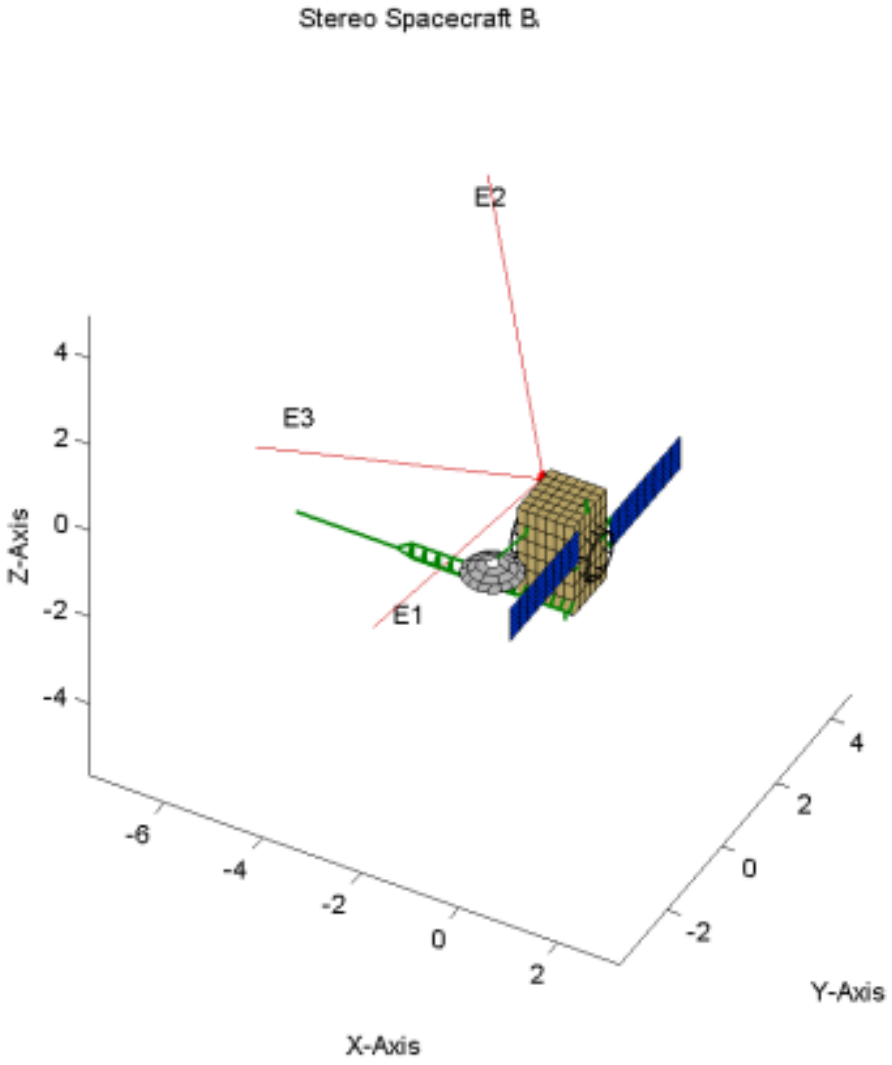


Figure 49: Spacecraft B

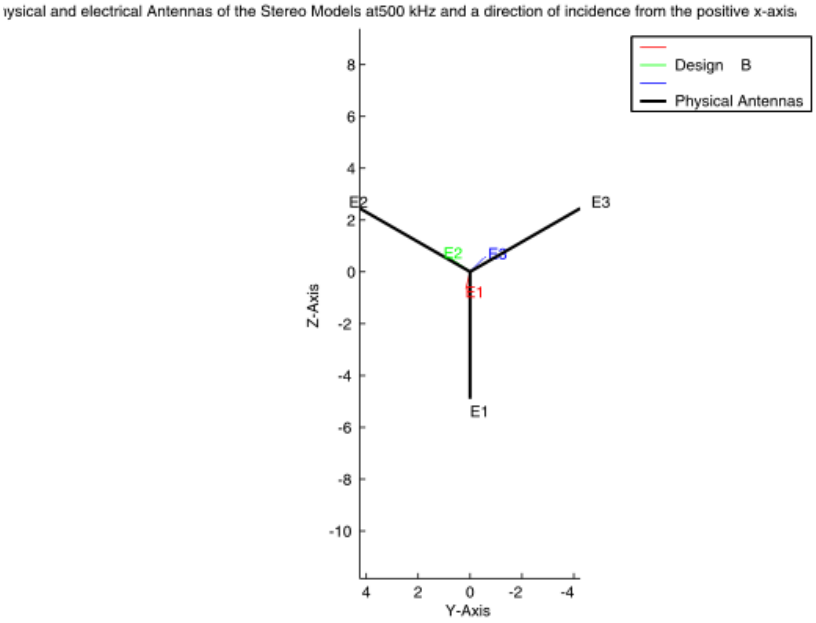


Figure 50: Spacecraft B: Effective Length Vectors,X-View/ Capacitances included

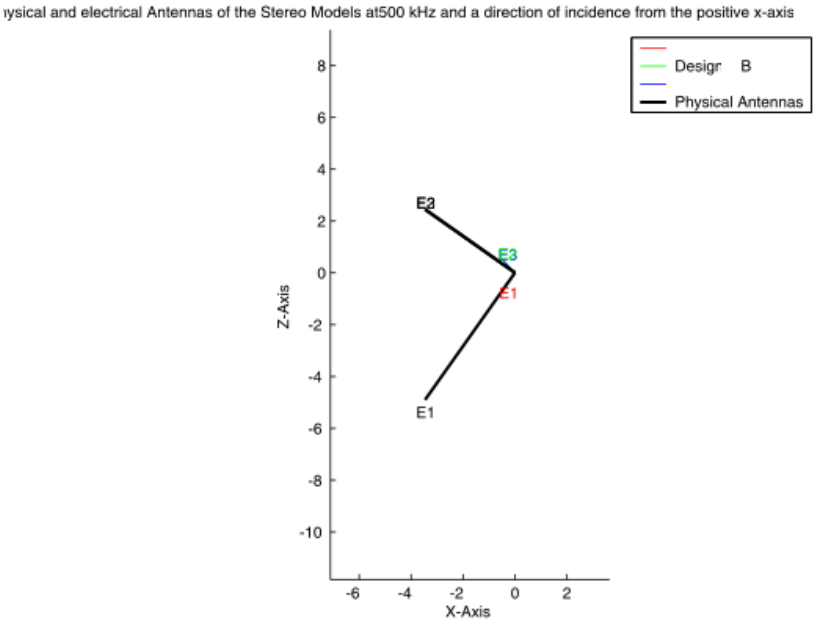


Figure 51: Spacecraft B: Effective Length Vectors,Y-View/ Capacitances included

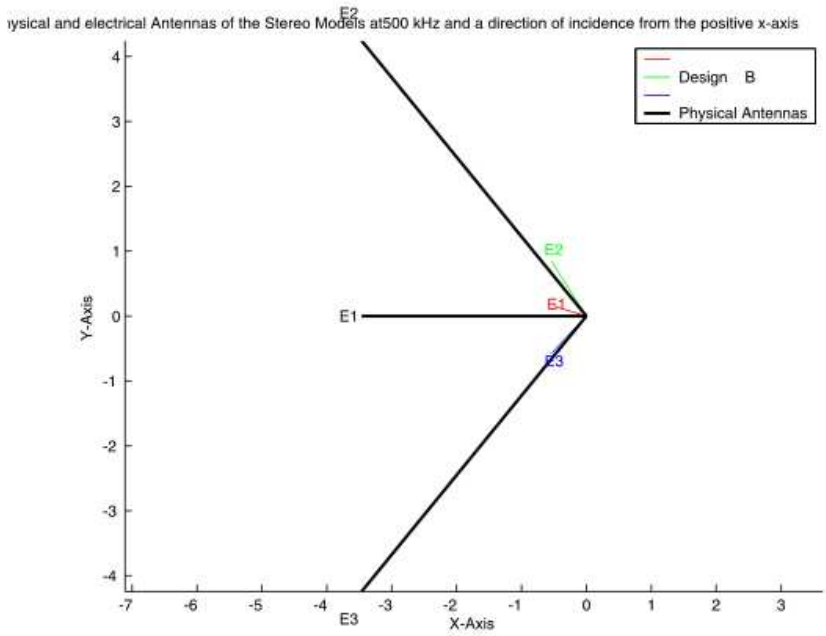


Figure 52: Spacecraft B: Effective Length Vectors,Z-View/ Capacitances included

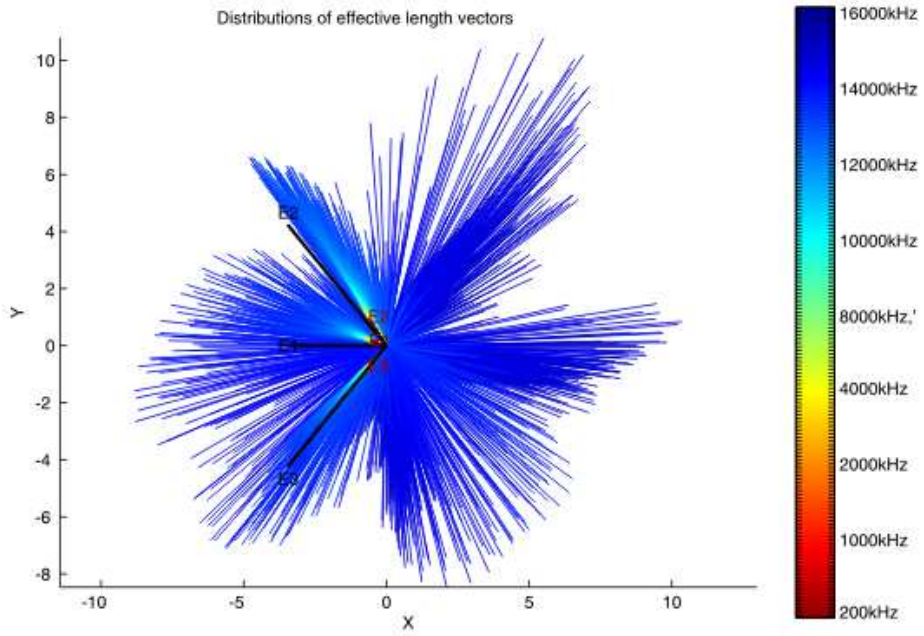


Figure 53: The spatial distribution of the real parts of the effective length vectors of the design 1 model B with capacitances included-16MHz/Z View

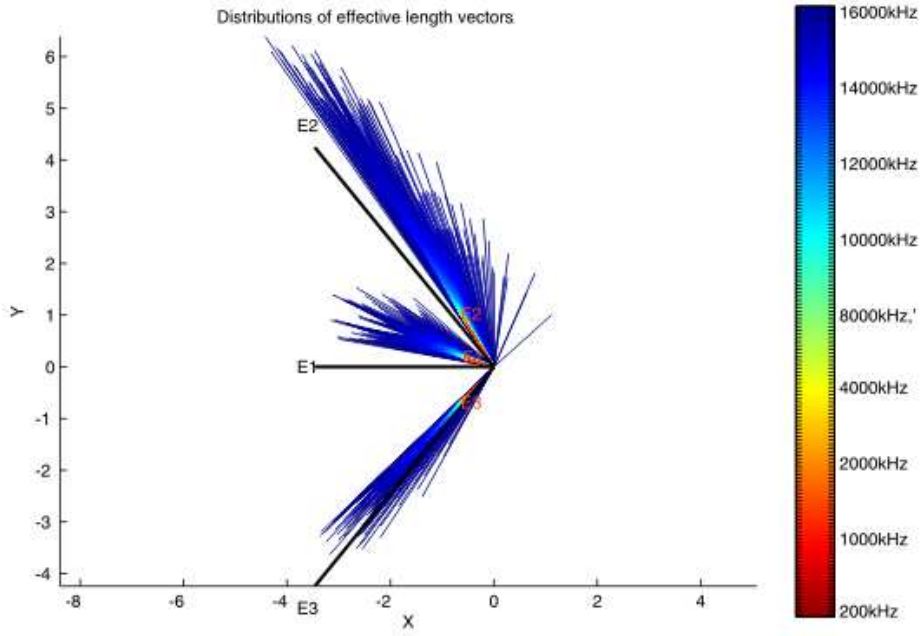


Figure 54: The spatial distribution of the real parts of the effective length vectors of the design 1 model B with capacitances included-13MHz/Z View

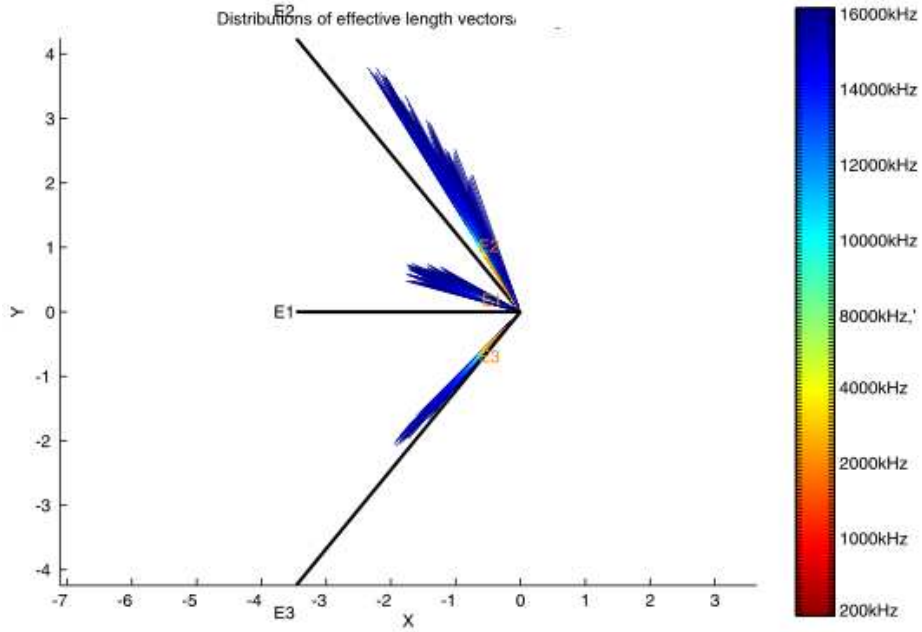


Figure 55: The spatial distribution of the real parts of the effective length vectors of the design 1 model B with capacitances included-12MHz/Z View

The quantitative plots are shown in figures 56 and 57. For comparison, the solutions of spacecraft A are plotted by using dashed lines.

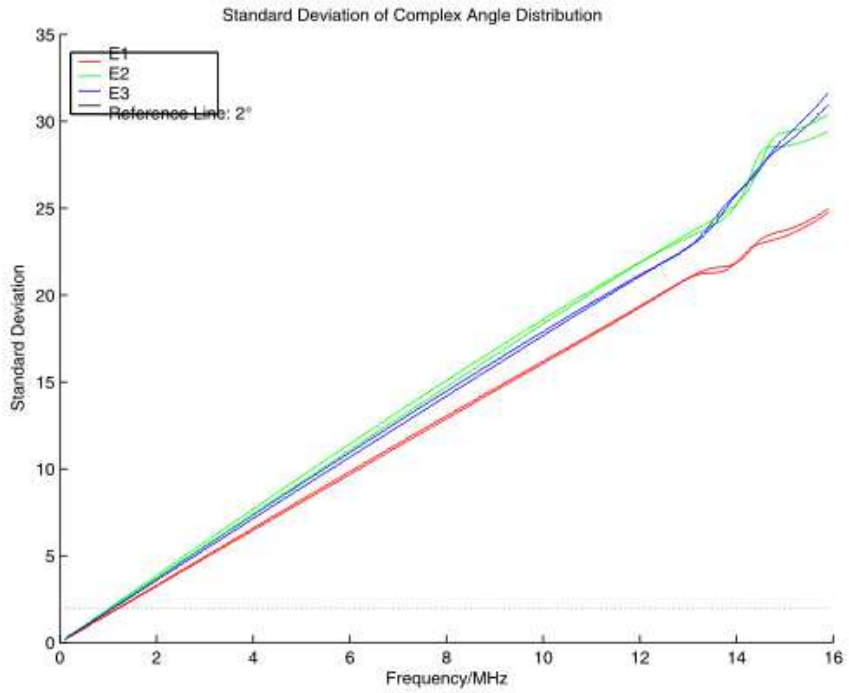


Figure 56: Standard deviation of the length, spacecraft A (dashed line) and B (full line)/capacitances Included

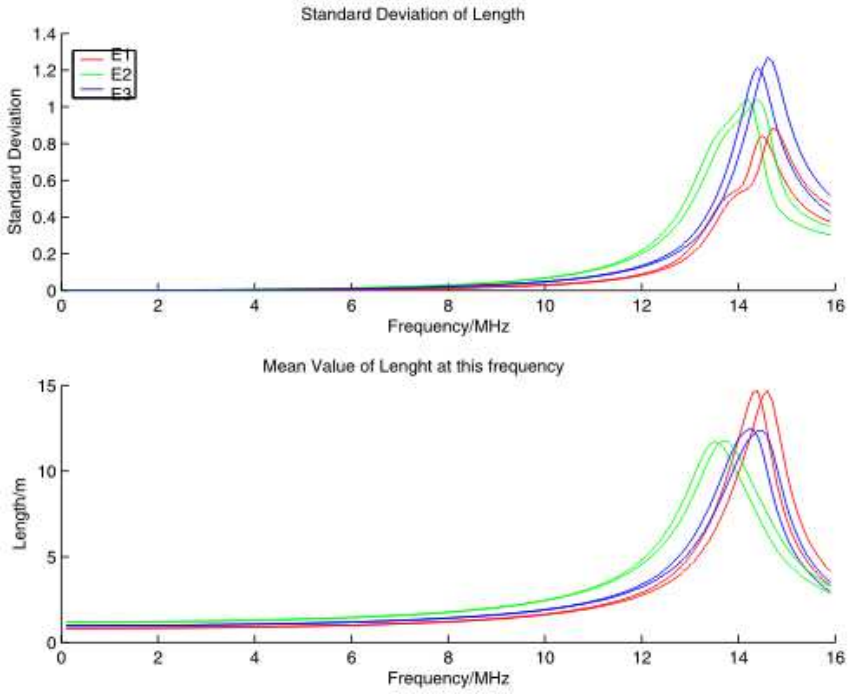


Figure 57: Complex standard deviation of the angular distribution, spacecraft A (dashed line) and B (full line)/capacitances included

## 7.2 The Covariance Matrix

The covariance matrices at frequencies of 500kHz and 1MHz are

$$10^{-9} \cdot \begin{pmatrix} \mathbf{9.334} & -6.884 & -8.201 & -135.0 & 76.76 & -189.4 & 1.641 & -74.17 & -57.16 \\ -6.884 & \mathbf{46.80} & -7.603 & -132.0 & -186.7 & 116.3 & -30.78 & 387.1 & -84.76 \\ -8.201 & -7.603 & \mathbf{23.80} & 241.1 & -71.71 & 358.8 & -44.41 & -85.56 & 127.3 \\ -135.0 & -132.0 & 241.1 & \mathbf{3500} & -592.6 & 3533 & 73.09 & -881.2 & 1790 \\ 76.76 & -186.7 & -71.71 & -592.6 & \mathbf{1228} & -2182 & 26.52 & -1501 & -252.3 \\ -189.4 & 116.3 & 358.8 & 3533 & -2182 & \mathbf{6705} & -900.10 & 648.2 & 1694 \\ 1.641 & -30.78 & -44.41 & 73.09 & 265.2 & -900.1 & \mathbf{478.2} & 22.78 & 132.2 \\ -74.17 & 387.14 & -85.56 & -881.2 & -150.2 & 648.3 & 22.78 & \mathbf{3419} & -598.0 \\ -57.16 & -84.76 & 127.3 & 1790 & -252.3 & 1694 & 132.2 & -598.0 & \mathbf{1035} \end{pmatrix} \tag{7}$$

and

$$10^{-7} \cdot \begin{pmatrix} \mathbf{1.504} & -1.110 & -1.319 & -21.53 & 12.47 & -30.74 & .4189 & -12.01 & -9.079 \\ -1.110 & \mathbf{7.530} & -1.220 & -21.46 & -30.39 & 18.87 & -5.031 & 62.34 & -13.98 \\ -1.319 & -1.220 & \mathbf{3.833} & 38.63 & -11.66 & 58.02 & -7.247 & -13.61 & 20.48 \\ -21.56 & -21.46 & 38.63 & \mathbf{559.4} & -94.24 & 566.1 & 11.05 & -142.6 & 288.4 \\ 12.47 & -30.39 & -11.66 & -94.24 & \mathbf{201.5} & -356.2 & 44.28 & -245.1 & -38.87 \\ -30.74 & 18.87 & 58.02 & 566.1 & -356.2 & \mathbf{1091} & -150.0 & 107.7 & 270.2 \\ .4189 & -5.031 & -7.247 & 11.07 & 44.28 & -149.8 & \mathbf{77.16} & 1.853 & 21.74 \\ -12.01 & 62.34 & -13.61 & -142.6 & -245.1 & 107.7 & 1.853 & \mathbf{550.2} & -98.77 \\ -9.079 & -13.98 & 20.48 & 288.7 & -38.87 & 270.20 & 21.74 & -98.77 & \mathbf{167.1} \end{pmatrix} \tag{8}$$

## 7.3 Variation of the effective length vectors with frequency at fixed direction

The response of the antennas to waves incident from the positive x-direction. (see Fig. 58 - 60) The results of spacecraft A is plotted in dashed lines for comparison.

## 7.4 The impedances and admittances

Plots of the impedances are shown in Figures 61 and 62, plots of the admittances in Figures 63 and 64. The base capacitances were included in the calculation.

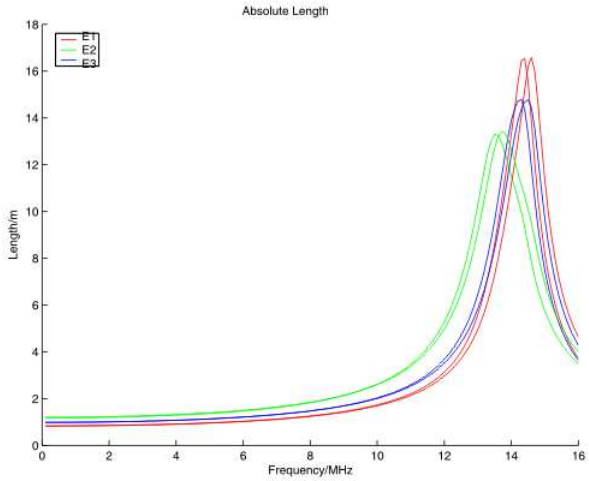


Figure 58: The absolute values of the coordinates of the electric antennas of the design 1 model B/Capacitances included

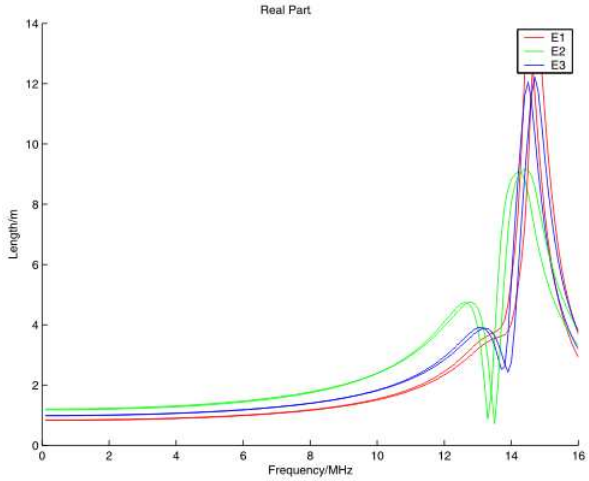


Figure 59: The real parts of the coordinates of the electric antennas of the design 1 model B/Capacitances included

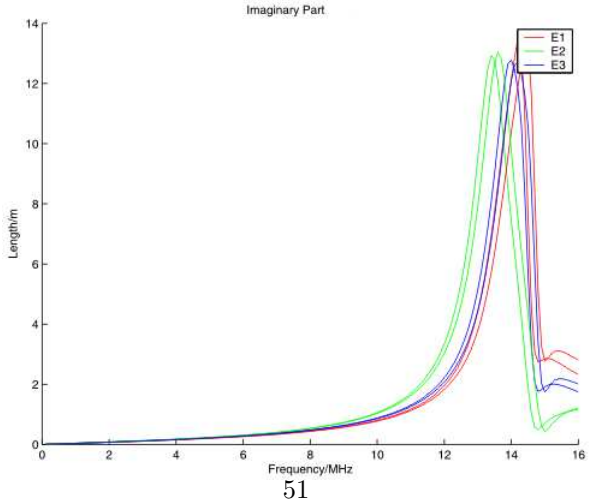




Figure 60: The imaginary parts of the coordinates of the electric antennas of the design 1 model B/Capacitances included

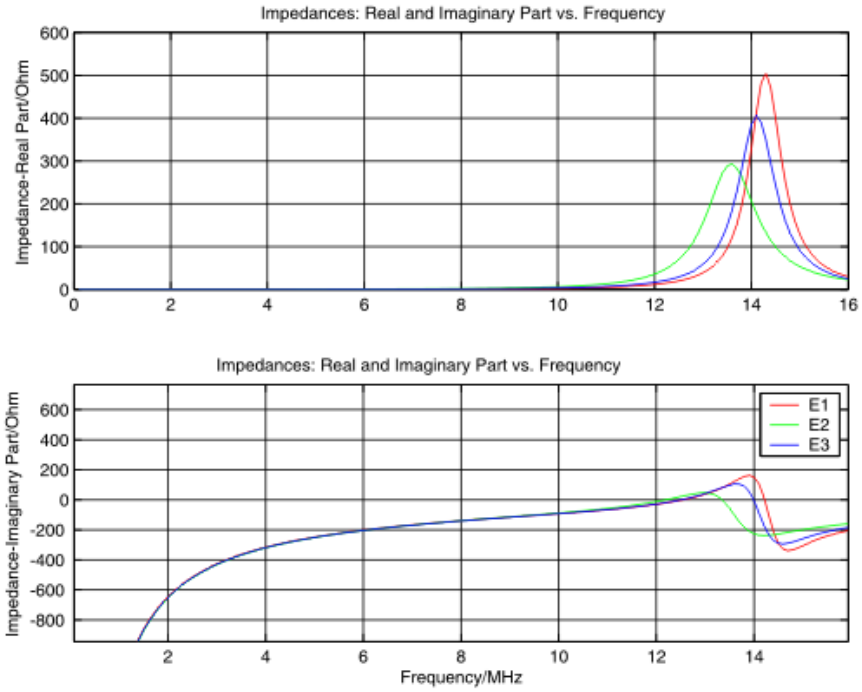


Figure 61: Impedances of design 1B, capacitances included

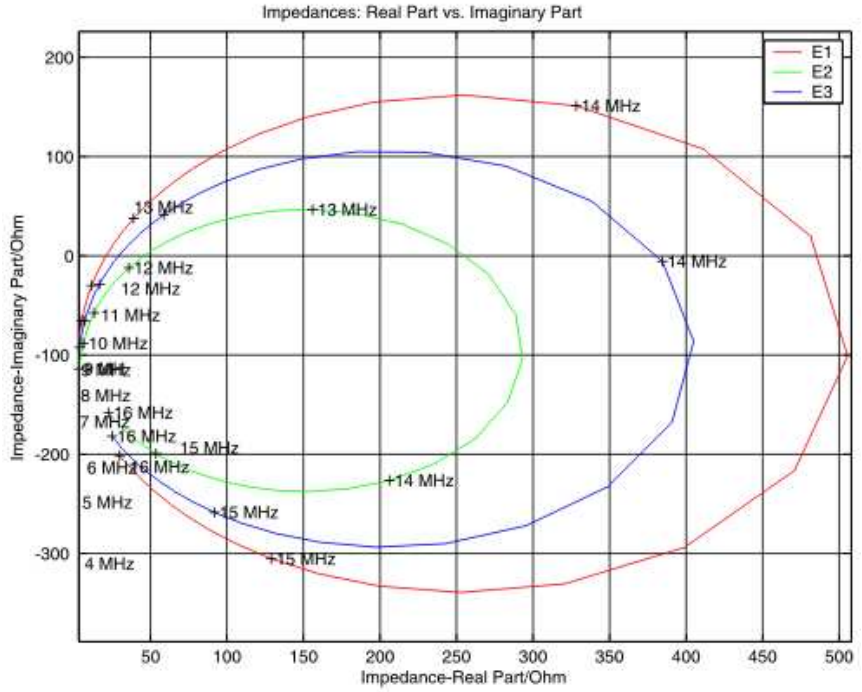


Figure 62: Impedances of design 1B, capacitances included

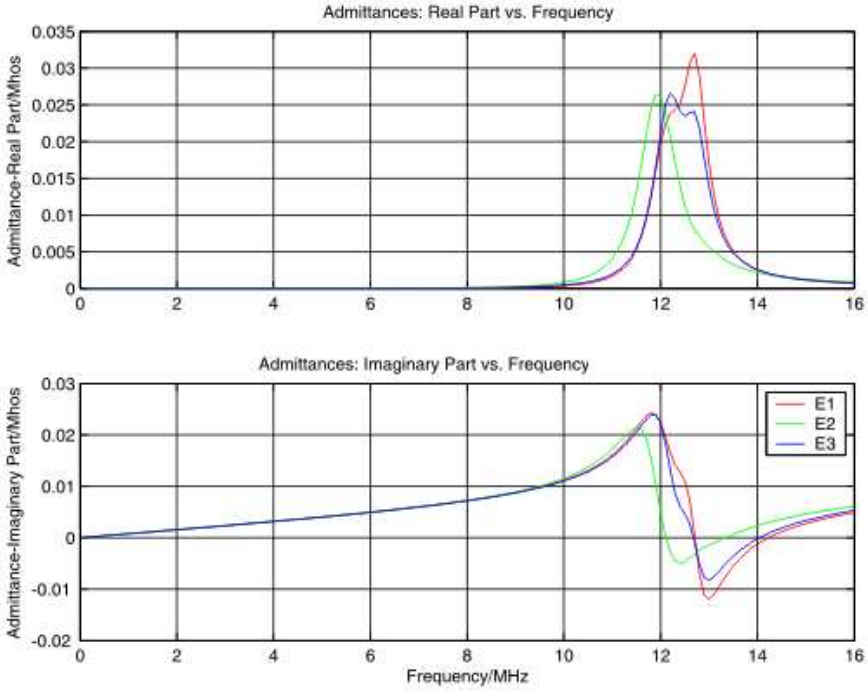


Figure 63: Admittances of design 1B, capacitances included

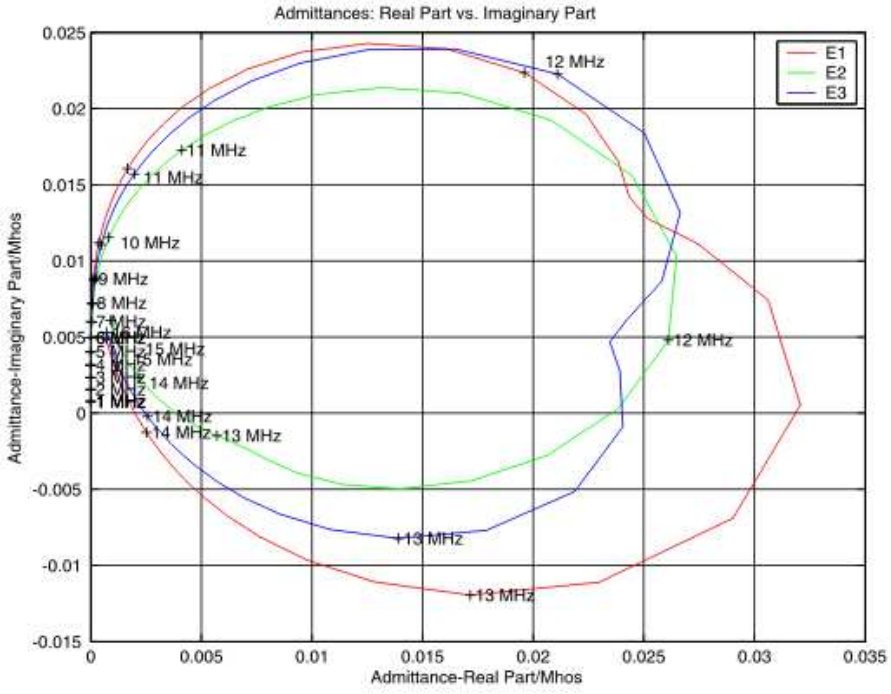


Figure 64: Admittances of design 1B, capacitances included

# 8 Appendix A: New functions: declarations

The matlab source code, used to produce the results presented in this report is based on the scripts, shown in the appendix of [1]. Small corrections had to be done in order to allow for the different coordinate frame used for design 1 and to include the capacitances. Please contact the authors of this report for details.

# 9 References

# References


[1] Oswald Th., W. Macher, G.Fischer, H.O. Rucker
First results of STEREO/WAVES Antenna calibration
Technical Report of the Space Research Institute/Austrian Academy of Science, 2004

[2] B.Cecconi, P. Zarka
Direction Finding and antenna calibration through analytical inversion of radio measurements performed using a system of 2 or 3 electric dipole wire antennas on a 3 axis stabelized spacecraft
March 2004

[3] Oswald Th. et. al.
Direction Finding as relevant for the
STEREO/SWAVES experiment